IN VITRO CYTOTOXICITY OF ^{198}Au-NPs LABELED HIV-1 Tat CPP FOR THE TREATMENT OF METASTATIC BREAST CANCER

A Thesis

by

ZAHER BASEL HAMOUI

Submitted to the Office of Graduate and Professional Studies of
Texas A&M University
in partial fulfillment of the requirements for the degree of

MASTER OF SCIENCE

Chair of Committee,	Gamal Akabani
Committee Members,	John Ford
	Michael Deveau
Head of Department,	Yassin Hassan

December 2015

Major Subject: Nuclear Engineering

ABSTRACT

The present research advances the area of targeted radionuclide therapy (TRT) by using nanoparticles as intrinsic carriers of radionuclides. In here we proposed the use of nuclear nanotechnologies where nanoparticle cores serve as super-carriers of radionuclides, potentially yielding new endo-radiotherapy agents with a higher safety and efficacy profile than those currently used in TRT. We studied a new original concept in TRT by introducing radioactive gold nanoparticles as carriers of the therapeutic payload while increasing the number of radioactive atoms per tumor cell. By separating the radionuclide from the targeting agent, it was possible to avoid the severe effects of radiolysis in molecular decomposition of the targeting agent, which is currently a limiting factor in TRT. We studied under this paradigm the beta-particle emitter ^{198}Au ($t_{1/2}$ = 2.69 d).

Using radioactive gold Au-198 ($t_{1/2}$ = 2.69 d) as a therapeutic load and the cationic cell penetrating peptide (CPP) HIV-1 Tat as a targeting agent, we developed the ^{198}Au-AuNP HIV-1 Tat as a therapeutic strategy for the treatment of breast cancer metastases. The breast cancer cell line SKBr-3 was used to test the cytotoxicity of ^{198}Au-AuNP HIV-1 Tat with different activity concentrations for an incubation time of 12 hours. The Real Time Cell Analyzer (RTCA) was used to quantitate the cell growth or delay as a function of time. When compared to controls, a delay in cell growth was observed for wells that were administered an activity of 1000 and 1500 kBq whereas no significant changes were observed for 50, 100 and 500 kBq. The effect of functionalized

^{198}AuNP-HIV1-Tat was observed to have a small effect in cell growth when compared with ^{198}AuNP alone.

Moreover, cell growth delay was compared with that obtained using external beam radiation therapy (2 Gy) and the chemotherapy agent doxorubicin. Results indicated that ^{198}Au-AuNP HIV-1 Tat at 5000 kBq was similar in toxicity to external beam therapy and lower than doxorubicin. We predict the use of cell penetrating peptides in combination with intrinsically radioactive nanoparticles as a new strategy against metastatic breast cancer.

ACKNOWLEDGEMENTS

My sincere gratitude is to my advisor Dr. Gamal Akabani for his continuous support, motivation, and patience throughout my undergraduate and graduate studies at Texas A&M University. Dr. Akabani taught me step by step, little by little, the many areas and tools used in nuclear medicine research, which have leaded me into pursuing a master's degree in this field. Dr. Akabani's guidance helped me in all the time of research and writing of this thesis, which will always be appreciated.

I would also like to thank the staff at the Nuclear Science Center for supporting this research, especially Jan Vermaak and Scott Miller for supplying us with much needed radioactive gold. I also want to thank the members of my committee, Dr. Michael Deveau and Dr. John Ford for their encouragement and insightful comments.

Finally, I would like to thank the Nuclear Engineering Department, especially the department head Dr. Yassin Hassan, Robb Jenson, and Marna Stephan for their support through my undergraduate and graduate studies.

DEDICATION

I dedicate my dissertation work to my family and friends that I am truly thankful for having them in my life, and will always appreciate all they have done.

A special feeling of gratitude is for my loving parents, Bassel and Dina who continuously encouraged and supported me through my entire incarnation and who have always loved me unconditionally and cared so much for me.

I dedicate this work and give special thanks to my uncle Hakam Madi and my aunt Luna Al Assi who have always cared for me, looked after me, and treated me like their son.

I also dedicate this thesis to my cousin, Naji Bayeh, who has supported me throughout the process, brought me joy and happiness, and was always there for me.

Last but not least, a very special feeling of gratitude goes to Mira Mirza who has never left my side and who has been a constant source of support and encouragement during the challenges of school and life.

TABLE OF CONTENTS

Page

LIST OF FIGURES

Page

LIST OF TABLES

Page

1. INTRODUCTION

1.1 Cancer Statistics

Cancer is a significant problem worldwide. A report by the World Health Organization (WHO) indicates that cancer will become, or already is, a global problem affecting third world countries disproportionately (1). As life expectancy increases around the world, the incidence of cancer continues to climb and it is expected to be the number one cause of death surpassing cardiovascular disease. It is estimated that there will be more than 25 million new cancer cases worldwide each year after the year 2025. Thus, cancer prevention and the development of individualized target therapies strategies must be given priority in order to minimize its societal burden.

According to SEER cancer statistics for the time period from 2005 to 2009, the average age at diagnosis for all type of cancers was 66 years. The age-adjusted incidence rate from 2005 to 2009 was 465.2 per 100,000 men and women per year and the median age of death from all type of cancers was 72 years (2). The age-adjusted death rate based on SEER statistics was 178.7 per 100,000 men and women per year (2).

1.2 The Prevalence of Cancer Metastases

The ability for tumor to metastasize makes cancer a fatal disease. A majority of cancer related deaths in the US can be attributed to metastatic disease progression rather than the primary tumor. At the time of diagnosis of cancer, at least half of the patients already present clinically detectable metastases. When a primary tumor is formed,

malignant cells in the primary tumor will tend to dissociate or release from the primary tumor mass, at an unknown rate, and travel in the body *via* the circulatory or lymphatic systems until they settle in a distant organ to develop secondary tumors. Unfortunately, a large portion of patients may already have developed clinically undetectable metastases or micro-metastases by current radiological or pathological techniques, at the time of diagnosis.

1.3 Current Therapies for Cancer

Currently, there are multiple approaches for cancer treatment depending on stage and disease progression. Surgery is considered to be the oldest and most effective strategy for tumors in early stages. The second strategy is chemotherapy. Historically, chemotherapy was introduced after World War I when nitrogen mustard was used to treat cancer (3). Chemotherapy is typically considered to be systemic treatment. Chemotherapy agents can be administrated intravenously or orally and they are commonly used along with surgery, external radiation therapy, or biological therapy (adjuvant therapy). Chemotherapeutics target non-specifically rapidly dividing cells using different mechanisms of action, depending on what aspect of the cell cycle and division they affect. However, chemotherapy can harm and affect healthy cells that naturally divide quickly, such as the stomach and intestines, bone marrow, and hair follicles. Fortunately, most of the side effects disappear few months post-administration.

After the discovery of x-rays by William Roentgen in 1895 the concept of external beam radiotherapy was immediately proposed. Today, approximately two thirds of all cancer patients treated in modern facilities will receive some form of radiation therapy as part of the cancer management plan. External beam radiotherapy is a complex treatment strategy, since it is grounded on the radiobiology of normal and tumor tissues (4). This modality is very effective against primary solid tumors and it requires a clear definition of the confined volume of the target and dose prescription. External beam therapy treatment consists of multiple treatment sessions to minimize acute and delay side effects to normal tissues while limiting the dose prescription to the tumor mass; unfortunately, once cancer disseminates and metastasizes to other organs and tissues, external beam radiotherapy is ineffective.

Brachytherapy is a modality that is similar to external beam radiation therapy, which uses sealed radioactive sources that are permanently implanted or localized temporarily within, or proximal to, a tumor tissue. The idea of using sealed sources to treat cancers was proposed initially by Pierre Curie, shortly after the discovery of radioactivity in 1896. This modality requires that the target tumor volume be well defined or the source be confined within a tissue. The sealed sources used in brachytherapy must generate a steep dose gradient in order to confine the dose to the tumor volume. The radioactive sources commonly used in brachytherapy are iodine-125 (^{125}I), cesium-137 (^{137}Cs), cobalt-60 (^{60}Co), Iridium-192 (^{192}Ir), palladium-103 (^{103}Pd), ruthenium-106 (^{106}Ru). Brachytherapy is further divided according to source placement, intensity of dose rate, and total dose. Brachytherapy has been used effectively in treating

localized prostate, breast, skin, cervical, oral, soft tissue sarcomas, gynecological and other cervix, head and neck, and central nervous cancers.

As with external beam radiotherapy, the use of brachytherapy can also induce deleterious side effects to normal tissues; therefore, careful treatment planning must be carried out in order to avoid severe side effects. Both external beam radiation therapy and brachytherapy require that the tumor be anatomical well confined within a region or organ and be geographically limited; however, when tumor progression occurs and a tumor disseminates beyond the primary site, such treatment modalities cannot be employed effectively. Therefore, other systemic treatment strategies, such as chemotherapy, must be used.

Advances in understanding cancer biology, the immunological system, and the differential expression of cell surface receptors between cancer and normal cell types has allowed the advancement of a group of strategies known as ‘targeted therapies’ in the treatment of cancer using drugs that exploit these differences between normal and tumor cells. Paul Ehrlich originally suggested the concept of targeted therapy in the early 1900s (5), this approach has gained particular attention in the last 20 years, since the advent of the genomic revolution (6). Targeted therapies, including cancer immunotherapy, are historically rooted in principles of microbiology and immunology, and these two research areas today form the core basis for developing new biological anticancer agents (7). The development of these agents has come about by understanding the cascade of events, commonly referred as the “signal transduction cascade” (8, 9), that are triggered by cell surface receptors and other cell-to-cell communication mechanisms or pathways.

These events induce a cell to carry out a specific task, such as proliferation, invasion, or migration, by secreting proteins capable of, for example, degrading the extracellular matrix of normal tissues for invasion purposes or induction of angiogenesis (formation of new blood vessels). The obstruction or inhibition of these cellular processes by specific biological drugs has shown to be effective in certain type of cancers. These drugs affect or interfere with the cascade of signals that are transmitted once a receptor is activated at the surface of the cell. The most significant of these biological drugs has been the humanized monoclonal antibody (mAb) trastuzumab (Herceptin®) for the treatment of breast cancer. This humanized mAb blocks the human epidermal growth factor receptor 2 (HER2) that is involved in the signal cascade associated with cell proliferation, migration, and invasion (10). Other therapeutics directed against or targeted at inhibiting a specific cellular process or protein target (*e.g.*, kinases) of relevance to tumor proliferation have also been developed (8). These drugs, referred to as inhibitors, often are small molecules compared to antibodies (11), some of which have shown considerable success in treating or controlling disease progression.

1.4 Targeted Radionuclide Therapy (TRT)

The employment of the combination of a high specificity immunotherapeutic agent with a radionuclide to effect targeted and localized killing of tumor cells, commonly referred as targeted radionuclide therapy (TRT) (5), has shown particular promise. The intent of radiation therapy is to use ionizing radiation to kill cancer cells by inducing cell death; in this manner it will stop these cells from growing and dividing.

One of the most applied methods that involve exposing patients to radiation is the external beam radiation therapy. This method uses multiple beams of high energy x-rays that irradiate a bounded area of the body, thereby concentrating the absorbed dose to the tumor tissue while minimizing the dose to normal surrounding tissues.

On the other hand, TRT uses a molecule, such as a monoclonal antibody, that attaches to antigens or receptors that are either over-expressed or located only on the surface of tumor cells. This molecule is labeled with a radionuclide in order to deliver a toxic level of radiation to both localized and disseminated disease sites scattered around the body. Unlike tumor-directed drugs and toxins, which kill only the targeted cells, an attractive feature of radionuclides is that their radiative emissions (beta and alpha particles) can exert a "crossfire" effect, potentially destroying adjacent tumor cells even if they do not over-express the specific tumor-associated antigen or receptor. Furthermore, TRT has the exclusive potential to eliminate both tumor cells at the primary tumor site and tumor cells that have spread throughout the body (metastases), including malignant cell populations that are clinically undetectable by radiographic imaging (commonly referred to as minimal residual disease).

Generally, the radio-therapeutic agent has two components: a radionuclide and a carrier that specifically attaches to tumor cells. Examples of molecular carriers are peptides, which seek and attach to their corresponding cell-surface receptors, and monoclonal antibodies, which attach to antigens that are expressed on the cell surface of tumor cells. The radionuclide that is attached to the carrier molecule can be chosen for its specific radiological characteristics, such as decay scheme, type of emitted radiation

(*e.g.*, alpha, beta, or gamma emitter), radiation range in tissue, and physical half-life. It is this modularity, where the components can be varied like interlocking building blocks, which allows the matching of the spatiotemporal pathophysiology specific of a tumor.

This strategy has been studied considerably for the last two decades. So far, the Food and Drug Administration has approved three TRT agents. The first two agents; namely, ^{131}I-labeled tositumomab (BEXXAR®, GlaxoSmithKline) and ^{90}Y-labeled ibritumomab tiuxetan (Zevalin®, Spectrum Pharmaceuticals, Inc.) were approved for the treatment of Non-Hodgkin's lymphoma (NHL) in the year 2003 and 2002, respectively. A third TRT drug, ^{223}RaCl (Alpharadin®), was recently submitted to the FDA for approval and it is prescribed for the treatment of bony metastases from castration resistant advanced prostate cancer (CRPC). The radionuclide ^{223}Ra is an alpha particle emitter with a physical half-life of 11.435 days. The approval of these agents has considerably boosted the research area of targeted radionuclide therapy, specifically, radioimmunotherapy. Currently, there are more than one hundred clinical trials using radioimmunotherapy as a treatment strategy.

Despite its advantages, TRT suffers from significant drawbacks. When a chemical or biological compound is radiolabeled, the "conjugate" (as it is commonly referred to) may dissociate due to ineffective chemical binding (ionic *vs*. covalent bonds), or it may become defective due to the high energy deposited by the radioactive substance into the sample (a process commonly referred as radiolysis). Therefore, only a fraction of the agent is labeled with a radionuclide and, in many instances, it is less than

5%. These are limitations that need to be resolved in order to enhance the effectiveness of TRT.

There have been many failures in seeking new TRT strategies, specifically for solid tumors and minimal residual disease settings. Many antigens have been tested as targets, using intact monoclonal antibodies or fragments. Several such targets have been found to be of little value, due either to low receptor expression or to extensive shedding into the blood stream, which make it almost impossible to specifically target the tumor sites themselves. Shedding interferes with targeting efficiency because of the depletion of radioactively labeled antibodies by circulating antigens, with subsequent uptake and degradation by the reticuloendothelial system (RES; liver, spleen). For example, the carcinoembryonic antigen (CEA), which is over-expressed in in patients with colorectal carcinoma, gastric carcinoma, pancreatic carcinoma, lung carcinoma and breast carcinoma, as well as individuals with medullary thyroid carcinoma, appears in blood in soluble form, and its high levels in blood compromises the binding of TRT agents to tumor cells (12). On the other hand, the CD20 antigen, which is over-expressed in all B-cell lymphomas, is an excellent target because it is neither shed in blood nor internalized by tumor cells (13).

The current trend in the pharmaceutical industry is to develop new therapy strategies capable of modifying the pathophysiology of tumors and the pharmacokinetics and pharmacodynamics (PK/PD) of existing drugs. This is accomplished by combining therapies for different cellular targets and with different mechanisms of action, that affect the survival and cell division of tumor cells. A large body of clinical evidence

supports the use of combined modality approaches based on the combination of ionizing radiation with known therapeutic molecules. The additive and synergism resulting from the combination of radiation and cytotoxic drugs has been shown in many clinical cases (14). However, in many other instances, combination therapies utilizing radiotherapy fail to show an additive or synergistic response (15, 16). The fundamental cause for such failure seems to be that they are spatiotemporally mismatched, as both therapies do not present themselves simultaneously to individual tumor cells at the correct time window and above a specific threshold concentration level (therapeutic dose), and that similar to efficacy, this may result in potential additive or synergistic toxicities. Therefore, basic to the use of a combined multimodality treatment is an understanding of the individual spatiotemporal effects of radiation and drugs and their combined interaction.

This area of combination therapy represents an important niche in translational cancer research. In order to address this niche, our labs are developing a new paradigm, referred to as nuclear nanotechnologies, that combines novel nanoparticles (*e.g.*, gold, polymeric nanoparticles) with radioimmunotargeting strategies to create spatiotemporally matched combination therapies.

1.5 Radioactive Nanoparticles in TRT

In traditional targeted radionuclide therapy, one radioactive atom is attached to one targeting agent (*i.e.*, monoclonal antibody). Typically, the efficiency (labeling yield) for radionuclide labeling is quite low, with labeling fractions ranging from 10^5:1 to 10^3:1 (unlabeled *versus* labeled antibody). However, a potential increase in efficacy can be

achieved by significantly increasing the payload per target agent. Our research is aimed at exploring the enhancement of therapeutic efficacy by the combination of immunotargeting and nuclear nanoparticle technologies.

Radioactive nanoparticles can carry not only a radioactive payload but also a biological modifier and/or a cytotoxic drug that can be spatiotemporally offered 'simultaneously' to each individual tumor cell. The use of nanocarriers transporting multiple payloads avoids issues of mismatched spatiotemporal effects, potentially inducing an additive or synergistic therapeutic effect to individual tumor cells. Although this is not a new concept, it is an approach that needs to be carefully studied at the *in vitro* and *in vivo* translational levels (17).

Nanoparticle technologies offer many advantages in comparison to traditional drug design and delivery methods (18). Nanocarriers can impact cancer treatment by improving the general pharmacokinetic (PK) properties of drugs, by increasing their solubility, retention, and tumor bio-distribution, and by providing multi-functional capabilities. As a consequence, there is a significant reduction in toxicity and an increase in efficacy. A typical clinical example is the chemotherapy drug Doxil (doxorubicin HCl liposome injection). Doxorubicin is a powerful anthracycline antibiotic used as a chemotherapy agent that works by intercalating DNA. Doxorubicin (Doxil) alone produces severe cardiac toxicity; however, when formulated as a liposomal drug, its solubility increased considerably while cardiac toxicity was reduced significantly. Doxil has been, and continues to be, used as a drug model for other nanotherapeutics (19).

Despite the advantages of nanoparticles, radioactive nanoparticles research for cancer therapy has been limited. This is due to difficulties in producing radioactive nanoparticles using synthetic methods under tracer conditions or complications with stabilizing nanoparticles (20). As an example, the generation of ^{198}Au nanoparticles (^{198}AuNPs) under physiological conditions using nontoxic agents in the presence of a functionalizing biomolecule, such as a monoclonal antibody, is still a major challenge. The challenges for the generation of radioactive NPs include:

a) Developing a method for the synthesis of radioactive NPs in isolation while avoiding NP aggregation.
b) Stabilization of radioactive NPs in a desired functional form (such as PEGylation).
c) Functionalization (*i.e.*, immuno-conjugation) of an active targeting agent to the stabilized radioactive NPs while maintaining its immunological properties under extreme physiological conditions, such as those encountered in the tumor microenvironment.
d) Prevention of an immunological response by the immune system and corresponding toxicity (21-24).

1.6 Cell Penetrating Peptides

The cell membrane is a biological barrier that encloses the cytoplasm of cells. This membrane act as a protection for the cell plasma that regulates what enters the cell depending on their molecular size. However, some of the drugs that are used for cancer

treatment are large enough to be blocked by the cell barrier. Therefore, an interesting method for the delivery of drugs of large molecules into the cell cytoplasm was discovered by the use cell penetrating peptides (CPP).

CPPs are divided into subgroups: protein derived (P), chimeric (C), and designed/synthetic (S). The most recognized CPPs is the (P) subgroup that is entirely derived from naturally occurring proteins such as HIV-1 encoded Tat protein. The main difference between chimeric and the designed/synthetic group is that the parental sequence in the chimeric group are partially naturally occurring peptide whereas the designed or synthetic group are unnatural and designed in laboratories.

The mechanism by which CPPs penetrate cells has not been fully elucidated. CPPs were discovered by Frankel and Pabo in 1988, who proved that that the transcription-transactivating (Tat) protein of HIV-1 can penetrate the cell membrane without causing significant damage (25). The CPPs are of various amino acids sequences and sizes. Today, they are commonly used in the field of cancer especially for breast cancer treatment. For example, by conjugating CPPs with a chemotherapy agent for a breast cancer treatment, the delivery of the drugs will efficiently increase. Figure 1 illustrate overview of applications for cell penetrating peptides (CPPs) for use *in vitro* and *in vivo*

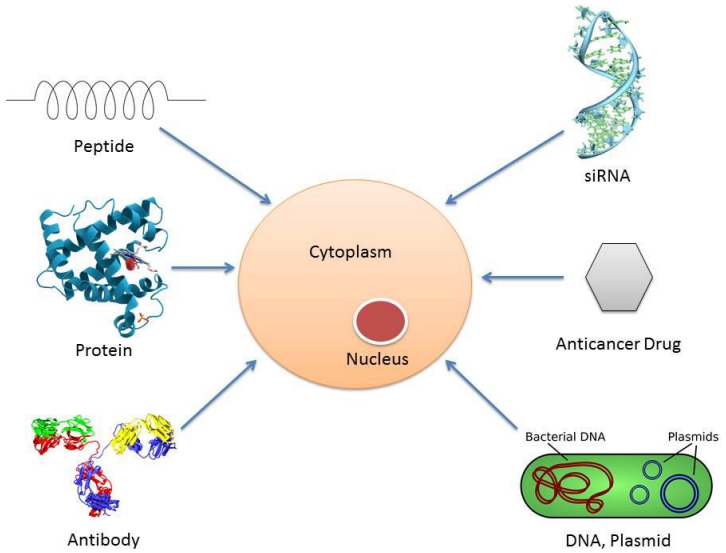

Figure 1. Overview of applications for cell penetrating peptides (CPPs) for use *in vitro* and *in vivo* (26). CPPs can be used to introduce peptides, proteins, antibodies, small interfering RNA (siRNA), small molecular weight drugs, plasmids and DNA.

1.7 Proposed Therapeutic Strategy

The present research explores a new paradigm of targeted nuclear nanotechnologies using the approach of immuno-targeted delivery of radioactive (^{198}Au) gold nanoparticles for the treatment of breast cancer in the SKBr-3 cell line and the potential of this strategy for the treatment of disseminated disease. The present strategy utilizes ^{198}Au as a cytotoxic agent embedded into a gold nanoparticle that is functionalized with a HIV-1 Tat CPP for its targeted delivery as illustrated in Figure 2. We have selected ^{198}Au for its simple production; however, ^{198}Au can be substituted for other radionuclides with potentially more advantageous radiobiological properties such as the Auger emitting radionuclide ^{125}I, or the alpha particle emitting radionuclide ^{211}At.

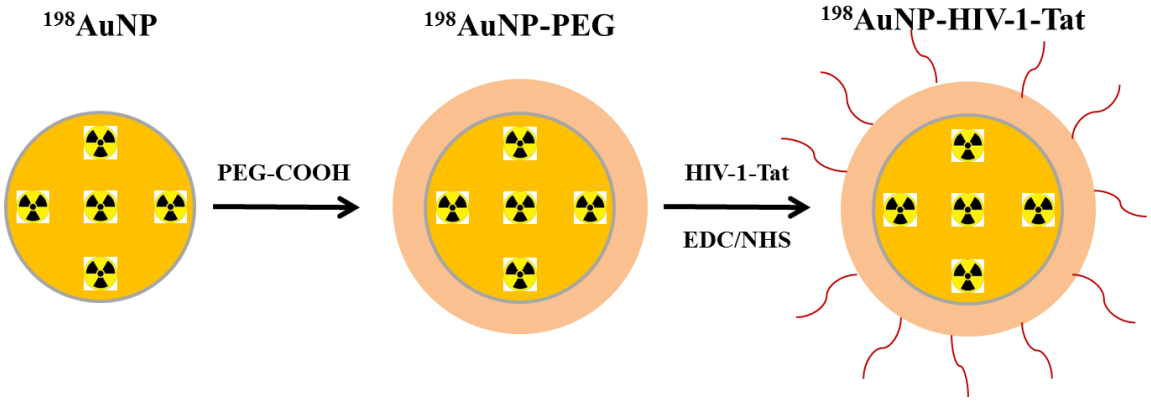

Figure 2. The proposed therapeutic strategy of functionalized ^{198}AuNp with a HIV-1 Tat CPP

2. METHODS

2.1 Cell Lines and Cell Culture

The breast cancer cell line SKBr-3 (ATCC Catalog No. HTB-30™) was obtained from American Type Tissue Culture (ATCC, Manassas, VA). This cell line was isolated and derived from the pleural effusion of a patient with breast adenocarcinoma at the Memorial Sloan-Kettering Cancer Center (MSKCC) in 1970. This cell over-expresses the HER2/c-erb-2 gene product producing an excessive number of HER2 receptors on the cell surface (25). The HER2 receptor has no natural ligand; however, a murine monoclonal antibody has been developed and humanized by Genentech, Inc. (27)

Cell culture was carried out according to the ATCC product information sheet. Briefly, the base medium used was ATCC-formulated McCoy's 5a Medium Modified (ATCC Catalog Number 30-2007) with 10% fetal bovine serum. No antibiotics were added to the growth medium. The SKBr-3 cell line was incubated in a 5% CO_2 atmosphere under sterile conditions. Sub-culturing and passage was carried out using 175 cm^2 flasks where the medium was removed and discarded and the cell layer was rinsed with the dissociating reagent TrypLE™ Express (Gibco®, Life Technologies, Grand Island, NY) for a period of 15 minutes or until cells detached from the surface of the flask. Cells were then aspirated into a 50 mL conical tube and 1 mL of the cell suspension was used to continue the propagation of the cell line into another new flask with 30 mL of fresh media. The remaining cells were then collected by centrifugation and used for experiments. Cell centrifugation was carried out at 100×g (relative

centrifugal force) for 5 min. The supernatant was discarded and cells were re-suspended in 5 mL of fresh growth medium at 37 °C for use in further experiments.

2.2 Real Time Cell Analysis (RTCA)

A label-free real-time cell analyzer (RTCA) was used to assess cell growth and cell-mediated toxicity of cytotoxic agents to attached cells. The xCELLigence RTCA DP analyzer (ACEA Bioscience, Inc. San Diego, CA) uses impedance measurement to assess the real-time response of attached cells to x-ray radiation, chemotherapeutics, and ^{198}AuNPs on SKBr-3 cells. The system has three plates and each plate has 16 wells that are continuously monitored by the system, providing a real time cell index response as a function of time. The cell index (CI) response has arbitrary units. Using experimental controls, the response of a cytotoxic agent can be estimated as a function of time. This system supersedes the use of the commonly used clonogenic assay (28), which only determines the potential for proliferation of cell *in vivo* as a function of absorbed dose or molar concentration.

The RTCA system requires the estimation of an optimal number of cells for seeding (per well) as to allow such cells to proliferate for a period time before treatment with a cytotoxic agent. In order to assess the optimal seeding per well, an initial experiment was carried out using various seeding numbers (3300, 5500, 10000, and 25000 cells per well). Once the optimal seeding number is established for SKBr-3, future experiments can be carried out for all pertinent cytotoxic agents.

2.3 Production of Radioactive Gold (^{198}Au)

Production of Au-198 was carried out at the Texas A&M University Nuclear Science Center (NSC). Briefly, 10 mg of high-purity gold (III) chloride trihydrate (Sigma Aldrich, St. Louis, Mo) in solid form was irradiated at the NSC for a minimum period of 4 h. Neutron activation of ^{197}Au resulted in the production of ^{198}Au *via* the reaction ^{197}Au(n,γ)^{198}Au. The thermal neutron cross-section is approximately 4916 barns. The activated solid sample was transported from the NSC to our labs using a compact shipment system for radioactive material (Model 001-724, Biodex Medical Systems, Shirley, New York). Upon receipt of the sample, an HPGe detector (Canberra Industries, Meridian, CT) was used to assess the radioactive purity of 198-Au and the presence of potential radioactive impurities or contaminants in the sample. A dose calibrator (ATOMLAB 500 Dose Calibrator, Biodex Medical Systems, Shirley, NY) was used to assess the net activity of the radioactive sample. The activity levels of ^{198}Au received varied considerably, depending on irradiation time at NSC and elapsed time for delivery.

The radionuclide ^{198}Au decays via beta particle emission and has a physical half-life of 2.6947 days with an average beta particle energy is 0.311 MeV. Table 1 presents the particle emission and abundances (yields) from ^{198}Au.

Table 1. Particle emissions and yields from the decay of ^{198}Au.

Radiations	y(i) (Bq-s)$^{-1}$	E(i) (MeV)	y(i)×E(i)
β- 1	9.86×10^{-03}	7.935×10^{-02} *	7.82×10^{-04}
β- 2	9.90×10^{-01}	3.146×10^{-01} *	3.11×10^{-01}
β- 3	2.50×10^{-04}	4.671×10^{-01} *	1.17×10^{-04}
γ 1	9.56×10^{-01}	4.118×10^{-01}	3.94×10^{-01}
ce-K, γ 1	2.87×10^{-02}	3.287×10^{-01}	9.43×10^{-03}
ce-L, γ 1	1.01×10^{-02}	3.970×10^{-01} a	4.00×10^{-03}
ce-M, γ 1	2.51×10^{-03}	4.082×10^{-01} a	1.03×10^{-03}
ce-N+, γ 1	7.40×10^{-04}	4.110×10^{-01} a	3.04×10^{-04}
γ 2	8.05×10^{-03}	6.759×10^{-01}	5.44×10^{-03}
ce-K, γ 2	1.74×10^{-04}	5.928×10^{-01}	1.03×10^{-04}
ce-L, γ 2	3.13×10^{-05}	6.610×10^{-01} a	2.07×10^{-05}
ce-M, γ 2	7.33×10^{-06}	6.723×10^{-01} a	4.93×10^{-06}
ce-N+, γ 2	2.21×10^{-06}	6.751×10^{-01} a	1.49×10^{-06}
γ 3	1.59×10^{-03}	1.088	1.73×10^{-03}
ce-K, γ 3	6.58×10^{-06}	1.005	6.61×10^{-06}
ce-L, γ 3	1.19×10^{-06}	1.073 a	1.28×10^{-06}
ce-M, γ 3	2.81×10^{-07}	1.084 a	3.04×10^{-07}
ce-N+, γ 3	8.41×10^{-08}	1.087 a	9.14×10^{-08}
Kα1 X-ray	1.37×10^{-02}	7.082×10^{-02}	9.69×10^{-04}
Kα2 X-ray	8.08×10^{-03}	6.890×10^{-02}	5.56×10^{-04}
Kβ X-ray	6.02×10^{-03}	8.030×10^{-02} *	4.83×10^{-04}
L X-ray	1.19×10^{-02}	9.990×10^{-03} *	1.19×10^{-04}
Auger-K	1.09×10^{-03}	5.380×10^{-02} *	5.84×10^{-05}
Auger-L	2.17×10^{-02}	7.600×10^{-03} *	1.65×10^{-04}
Listed X, γ, and γ$^{\pm}$ Radiations			4.03×10^{-01}
Listed β, ce, and Auger Radiations			3.27×10^{-01}
Listed Radiations			7.30×10^{-01}

* Average Energy (MeV).

[a] Maximum Energy (MeV) for subshell.

Mercury-198 Daughter is stable.

2.4 Production of Radioactive Gold Nanoparticles (^{198}Au-Nps)

Radioactive AuNPs were produced using the Turkevich method (29) as described by Kumar, *et. al*. (30) and Frens *et. al*. (31). Briefly, 1 mL of a 12.7 mM ^{198}Au chloroauric acid solution was added to 49 mL of deionized ultra-filtered (DIUF) H_2O in a clean 100 mL three-neck round-bottom flask fitted with a stir bar and reflux condenser. To this solution under reflux was added 0.94 mL of 38.8 mM trisodium citrate. The solution turned cherry red in *ca*. 2-3 min, after which refluxing was continued for 10 min, producing 50 mL of highly spherical, mono-disperse gold nanoparticles between 15 to 30 nm in diameter, depending on chloroauric acid concentration. Particles were characterized by transmission electron microscopy (TEM) and UV-Vis spectroscopy. Nanoparticle size may be altered by the timing of trisodium citrate addition to the flask (31). Nanoparticles were found to be stable for several months if stored at 4 °C.

2.5 Nanoparticle Characterization Using NanoDrop 2000C Spectrophotometer

Nanoparticles produced in our laboratory where compared with commercially available standards obtained from CytoDiagnostics, Inc. and came with a certificate for nanoparticle size and concentration. In order to find the size of the gold nanoparticles, each sample was measured using the Thermo Scientific NanoDrop 2000C spectrophotometer. From each sample, 1 mL was pipetted into the cuvette and measured to produce absorbance spectra as a function of wavelengths (Figure 3). The wavelength for each sample was compared to the standard and showed strong correlation; while the absorbance peaks were recorded for the calculation of the sample concentration.

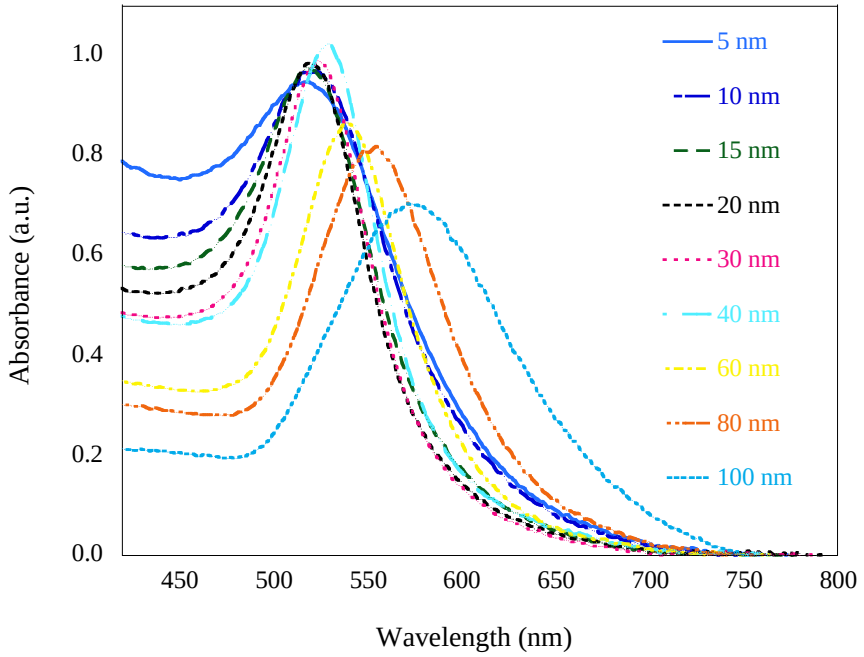

Figure 3. UV-Vis absorbance as a function wavelength (nm) for different AuNP standards of 5, 10, 15, 20, 30, 40, 60, 80 and 100 nm in diameter obtained using a spectrophotometer (NanoDrop 2000C, Thermo Scientific, Inc.).

The correlation between peak absorbance and nanoparticle size was plotted and fitted to a quadratic equation (Figure 4), where The relationship found was $A = 5.1602 \times 10^{2} + 1.1918 \times 10^{-1} D + 4.5615 \times 10^{-3} D^{2}$ with a correlation coefficient of R = 0.99905. In this matter, it was possible to assess the average particle size from any of our experiments producing radioactive gold nanoparticles.

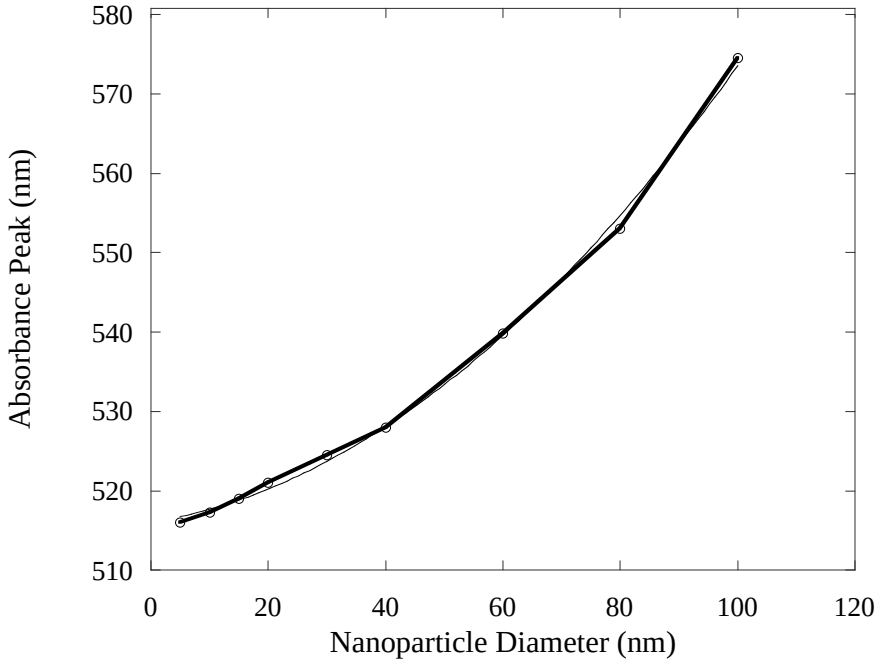

Figure 4. Absorbance peak as a function nanoparticle diameter obtained using different AuNP standards of 5, 10, 15, 20, 30, 40, 60, 80 and 100 nm.

The concentration of gold nanoparticles was calculated using the Beer-Lambert law expressed as

$$A = \varepsilon \cdot b \cdot C \tag{1}$$

where ε represents the extinction coefficients $\left(\mathrm{M^{-1}\ cm^{-1}}\right)$, b that is the path length (cm), and C is the concentration in the sample expressed in molar concentration (M), and A is the absorbance peak. Previously, the extinction coefficients, ε, were determined by Liu et al, (32) using UV-Vis spectroscopy for different particle sizes and surface ligands. In our case the surface ligand is trisodium citrate and the path length of our spectrophotometer is set at b = 1 cm. The nanoparticle concentrations from our samples produced in our laboratory were calculated using Eq. (1). The extinction coefficients as

a function of time estimated by Liu et al and those calculated using the standards showed high correlation as shown in Figures 5 and 6.

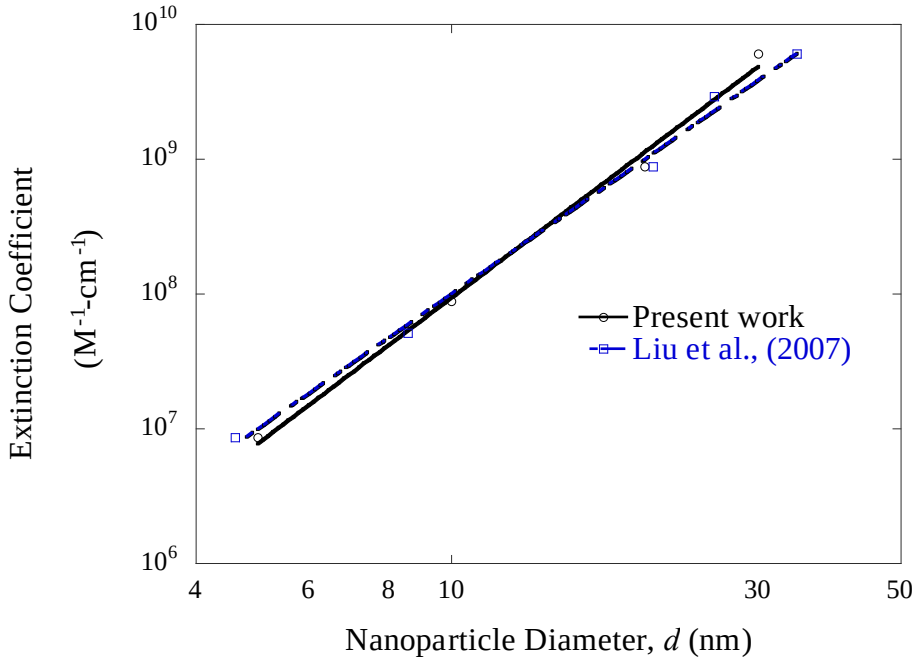

Figure 5. Extinction coefficient, ε, as a function of nanoparticle diameter, d, estimated by Liu et al., (32) and those calculated using the standards supplied by CytoDiagnostics, Inc. The correlation between them is in good agreement.

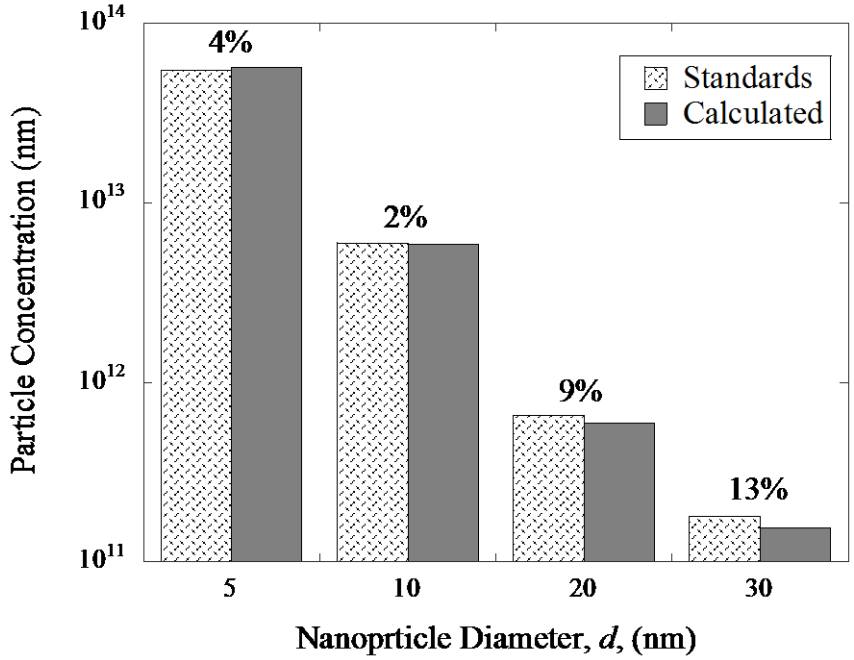

Figure 6. Comparison between gold nanoparticle concentrations obtained from standards versus those calculated using the extinction coefficient, ε, given by the equation established from Liu et al., (32). The difference between our standards and those calculated was within range.

2.6 Nanoparticle Characterization Using the NanoSight NS300

The NanoSight NS300 instrument was also employed in the characterization of the nanoparticles. The system uses laser diffraction to assess the random Brownian motion or tracks of nanoparticles in a viscous fluid and based on the Stokes-Einstein law the particle diameter is estimated. Again, the CytoDiagnostics, Inc. standards and their associated certificate for nanoparticle size and concentration were utilized. From each sample, 10 µL was introduced into the system and measured to produce normalized concentration spectra as a function of nanoparticle diameter as shown in Figures 7

through 10. The data from the spectra were then analyzed to find the diameter size of the nanoparticles.

The calculated diameter sizes were compared to the standards where they showed moderate correlation. The nanoparticles diameter sizes for the 10, 15, 30, and 60 nm nanoparticles were measured to be 6.6, 17.6, 34.8, and 64.4 nm respectively.

There was a 34% difference for the 10 nm AuNP, 17.33 % difference for the 15 nm AuNP, 16.0% difference for the 30 nm AuNP, and 7.33% difference for the 60 nm AuNP.

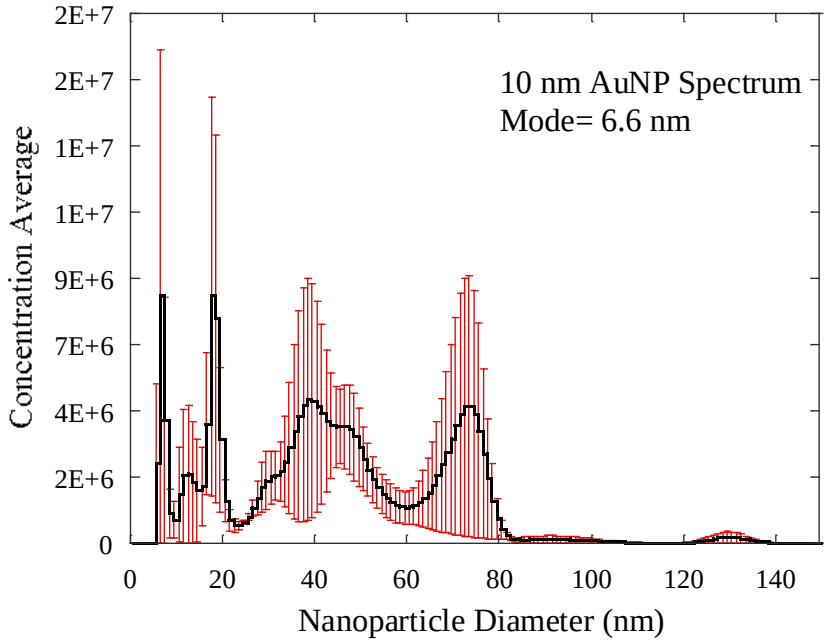

Figure 7. The average concentration as a function nanoparticle diameter (nm) for AuNP standard of 10 nm diameter obtained using the NanoSight NS300 instrument.

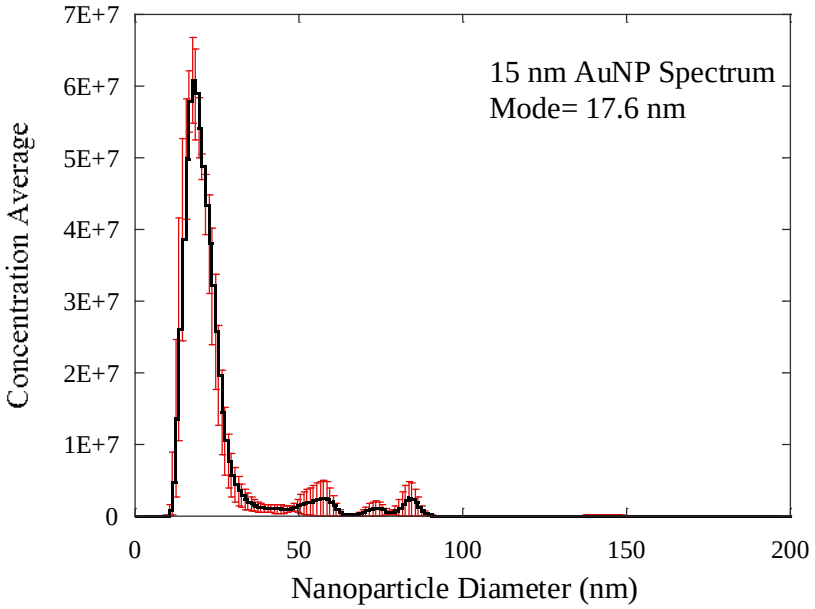

Figure 8. The average concentration as a function nanoparticle diameter (nm) for AuNP standard of 15 nm diameter obtained using the NanoSight NS300 instrument.

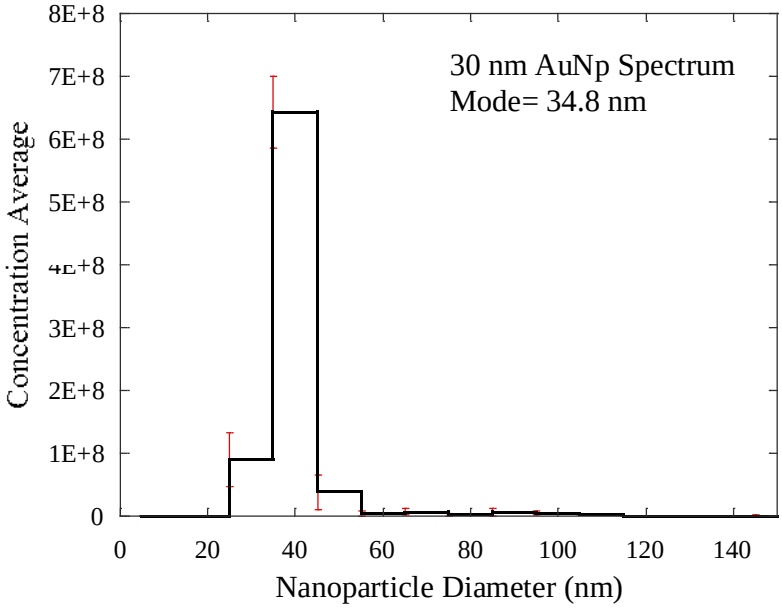

Figure 9. The average concentration as a function nanoparticle diameter (nm) for AuNP standard of 30 nm diameter obtained using the NanoSight NS300 instrument.

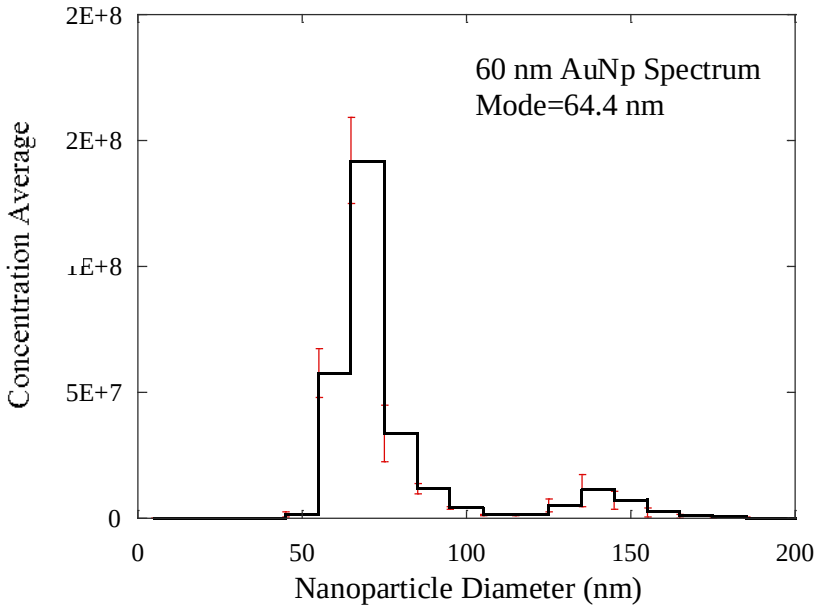

Figure 10. The average concentration as a function nanoparticle diameter (nm) for AuNP standard of 60 nm diameter obtained using the NanoSight NS300 instrument.

Using the data obtained from the NanoSight instrument, there was an observed inverse relationship between nanoparticle diameter and the error. This shows that the NanoSight instrument was not accurate for nanoparticles with a diameter smaller than 15 nm; therefore, it will be difficult to differentiate between a small diameter nanoparticle and a group of the same diameter nanoparticles.

2.7 TEM Image Analysis of AuNPs

Transmission electron microscopy (TEM) was used to characterize the shape, size, and particle number of AuNP. Reproducible synthesis of AuNP was confirmed by TEM analysis. Figure 11 (Top) shows the TEM images of AuNPs at different magnifications, which show well defined nanoparticles with little to no nanoparticle

fusion. Image analysis for nanoparticle diameter was carried out using the software program ImageJ (33). A narrow distribution for AuNP was obtained with a range between 11.6 and 23.5 nm and an average diameter of 15.9 nm (Figure 11 (Bottom))

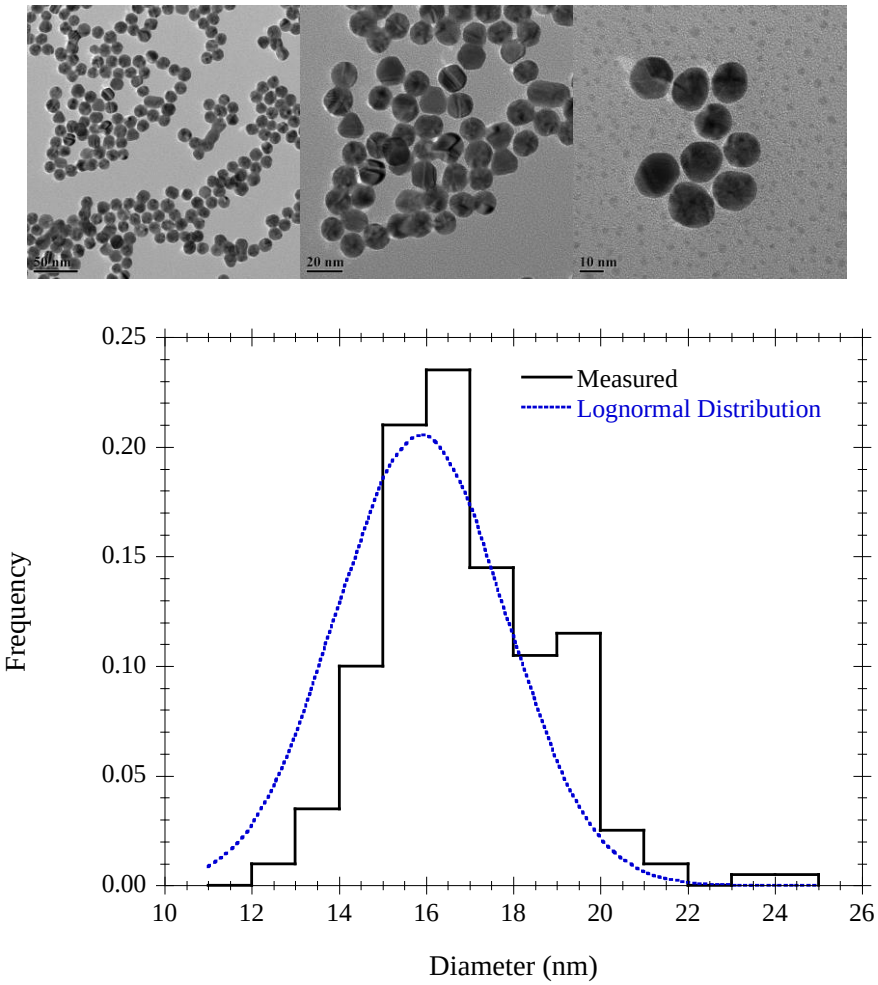

Figure 11. (Top) TEM images of AuNPs produced under the present method at different magnifications. (Bottom) Image analysis demonstrated a narrow particle size distribution, with a size range between 11.6 and 23.5 nm and an average diameter of 15.9 nm. A lognormal distribution was fitted to the data showing the negative skew of the measured distribution towards larger size nanoparticles.

2.8 Estimation of Number of ^{198}Au Radioactive Atoms Per Nanoparticle

Once radioactive NPs are generated using the Turkichev method, the total activity per unit volume (μCi/ml) was estimated using a dose calibrator (AtomLab 500, Biodex, Inc.). When a sample of solid chloroauric acid is activated, only a fraction of the ^{197}Au gold atoms are transformed into ^{198}Au. This reaction takes place via the ^{197}Au(n,γ)^{198}Au reaction. The fraction of atoms transformed into radioactive gold is very small when compared to the total number of atoms of gold in the sample and it depends on neutron irradiation conditions, such as neutron flux (n cm^{-2} s^{-1}), irradiation time, and decay (*e.g.*, due to delay in shipment). The nominal neutron flux used to irradiate our samples at the Nuclear Science Center was approximately 1×10^{13} n cm^{-2} s^{-1}. The specific activity of a radioactive sample is estimated using an HPGe detector. Specific activity is the total activity per unit mass of a compound; it is commonly expressed in MBq per mg.

The number of radioactive gold per nanoparticle follows the Poisson distribution and depends on the average NP size and specific activity. For example, larger particles may contain more radioactive atoms and *vice versa*. The diameter distribution obtained from TEM images (Figure 11) was used to carry out these calculations and convoluted with Poisson distribution. The average activity (Bq) per nanoparticle, A_{NP}, is the product of the NP mass multiplied by the specific activity, *SA*, where

$$A_{NP} = V_{NP} \cdot \rho \cdot SA = \frac{4}{3}\pi {r_{NP}}^3 \cdot \rho \cdot SA \tag{2}$$

where r_{NP} is the radius of a nanoparticle. The average number of radioactive atoms per nanoparticle, N_{NP}, is then given by

$$N_{NP} = \frac{A_{NP}}{\lambda} \tag{3}$$

where $\lambda = 2.98\times10^{-6}$ s is the decay constant of ^{198}Au . Thus the average number of radioactive atoms increases with specific activity *SA*. The probability of number of radioactive atoms per NP with a specific radius is given by

$$P(x) = \frac{\mu^x e^{-x}}{x!} \tag{4}$$

Where $\mu = N_{NP}$ is the average number of radioactive atoms in a nanoparticle. Thus, the fraction of radioactive atoms as a function of *SA* for a nominal NP diameter of 15.9 is given in Figure 12.

Once radioactive nanoparticles are produced, it is possible to assess the distribution of radioactive atoms per nanoparticle in a given solution using an estimate of the average diameter, nanoparticle concentration (NPs per milliliter), and activity concentration per unit volume of the sample. The average diameter can be calculated using the UV-Vis method; the concentration of NPs can be estimated using the optical absorption, and the activity concentration (not specific activity) using a dose calibrator. Therefore, we can write

$$\mu = \frac{1}{\lambda(s^{-1})} \frac{Activity\ Concentration, A\ (Bq\ ml^{-1})}{Nanoparticle\ Concentration, NP(NPs\ ml^{-1})} \tag{5}$$

and based on the Poisson distribution, the fraction of NPs with zero radioactivity atoms is given by $P0) = \mathrm{e}^{-\mu}$, similar estimates can be made for one radioactive and multiple radioactive atoms per nanoparticle.

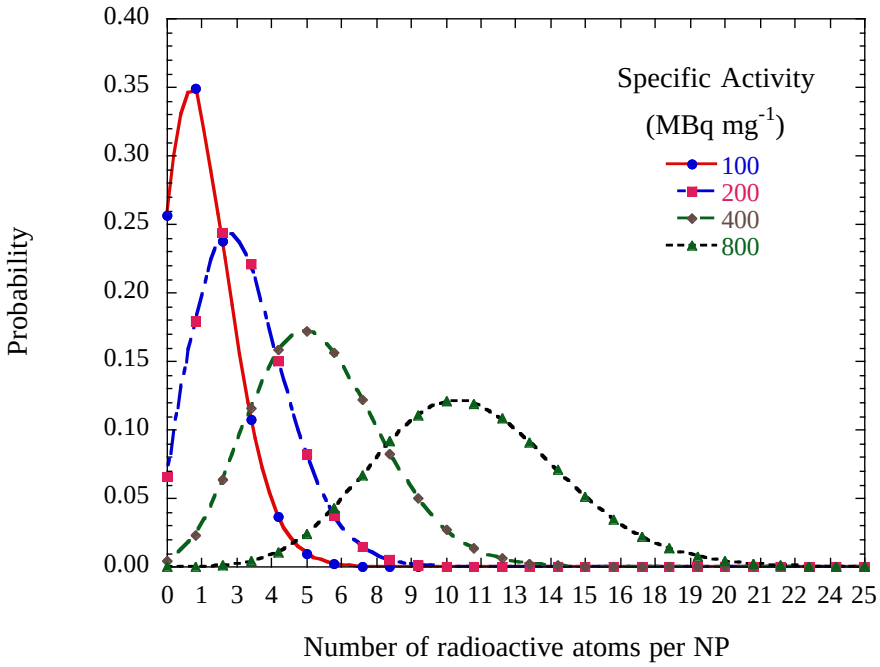

Figure 12. Poisson distribution showing the fraction or probability of having zero, one or more radioactive atoms of ^{198}Au per NP as a function of *SA* (MBq mg^{-1}). The fraction of NPs that will have a zero radioactive atoms decreases exponentially as a function of *SA*. The nominal NP diameter used in these calculations was 15.9 nm.

These calculations are required in order to assess how many radioactive atoms and corresponding decays will occur per NP. Each radioactive decay will emit certain characteristic radiative emissions based on the decay scheme of ^{198}Au. For a given NP, each radiative emission will occur in the same cell when the nanoparticle is entrapped in the cell surface or internalized in the cytoplasm, yielding a higher dose per tumor cell.

2.9 Pharmacokinetics and Dosimetry at the Cellular Level of ^{198}Au-NP HIV-1 Tat

The dosimetry of a single ^{198}Au-NP requires the use of the radiative emissions of ^{198}Au. The radionuclide ^{198}Au is a pure beta-particle emitter with multiple characteristic

gamma and x-ray emissions. The average energy of the emitted beta particles is 0.311 MeV with a maximum energy of 1.37 MeV (see Figure 13). The average range of these electrons in water was estimated at 0.099 cm, which is smaller than the size of a single well. There are also discrete electrons and x-ray emissions with significant intensities that contribute to the localized absorbed dose per radioactive decay.

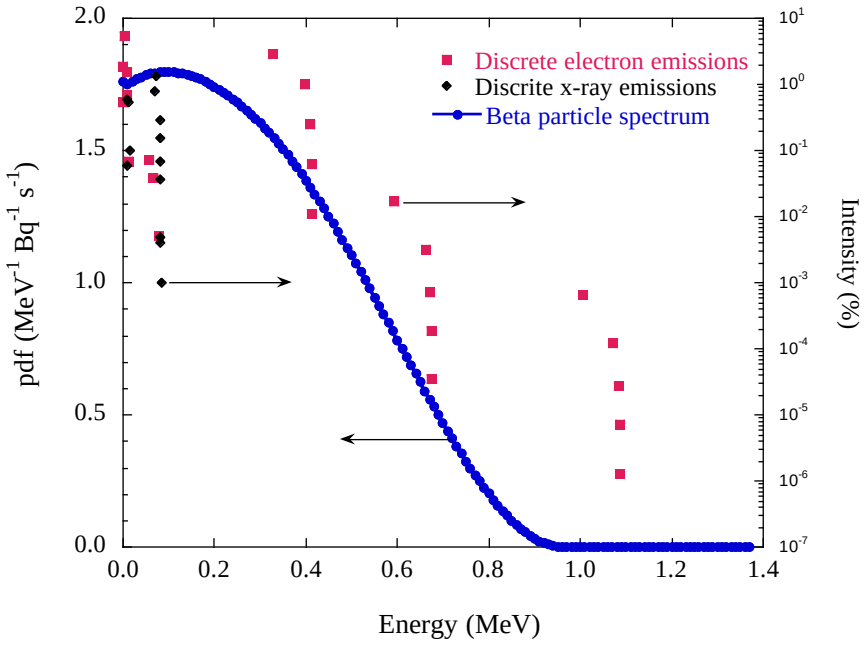

Figure 13. Probability density function (pdf) of the energy of beta particles emitted by the decay of ^{198}Au, and percent intensity of discrete x-ray and electron emissions. The energy of the emitted beta particle is sampled from this distribution.

The pharmacokinetic equations that govern the present system of cell growth are complex. We did not attempt to assess the absorbed dose to a single cell as the system is under continuous growth and requires a complex system of differential equations where radiation damage is transmitted to cell progeny. Nonetheless, it is important to mention

that radiation dosimetry of the present system as a bolus is not proper, as cell cycle continues to plays significant role and the distribution of radioactive nanoparticles that may not be homogenous among cells. Thus, the cumulative activity in the cell system will be based on cell growth, and internal nanoparticle micro-distribution among cells.

2.10 PEG Modification of ^{198}AuNPs

PEG (polyethylene glycol) modification, or PEGylation, is one of the most commonly used surface modification methods for gold nanoparticles. The PEG coating decreases the reduction of protein absorption and increases the stability of the AuNPs. The PEG modification was carried out in our laboratory using the methods described by Cytodiagnostic (Tech Note #105). Briefly, 1 mL (0.25 nmol) of AuNPs coated with citrate (1.5x1014 particles/mL) was PEGylated by simple ligand exchange of citrate with a 1000-fold molar excess of carboxy-PEG5000-thiol (CM-PEG500-SH, Laysan Bio) in DI water for 15 min. PEGylated carboxyl-terminal AuNPs (198AuNP-PEG-COOH) were collected by centrifugal filtration at 5000 x g using 10 kDa MWCO Amicon Ultra-15 centrifugal filter units (Millipore) to remove excess unreacted PEG reagents, repeatedly washed with DI water, and reconstituted in 0.5 mL MES buffer for immunoconjugation.

2.11 Functionalization Cell Penetration Peptide

Functionalization with the cell penetrating peptide of PEGylated radioactive gold nanoparticles was carried out using the method described by Cytodiagnostic

(Tech Note #105)[i]. Briefly, 30 mg of 1-Ethyl-3-carbodiimide hydrochloride (EDC) (Sigma, Cat# E1769) and 36 mg of N- hydroxysulfosuccinimide (Sufo-NHS) (Sigma, Cat# 56485) was mixed in 1 mL of MES buffer (Sigma, Cat# M5287) to form the EDC/NHS solution. *Conde et al.,* has described in detail the above functionalization method. The advantage of EDC coupling in the increase in water solubility of PEG-AuNPs, which allows for direct bio-conjugation without the prior use of an organic solvent to increase the stability of an active ester, such as N-hydroxysulfoxuccinimide (sulfo-NHS). The addition of sulfo-NHS stabilizes the amine-reactive intermediate by converting it to an amine-reactive sulfo-NHS ester; therefore, it increases the efficiency of EDC-mediated coupling reactions (34). The following steps were followed:

1. We prepared a fresh EDC/NHS mix solution, as described before, in MES buffer at a concentration of 30 mg/mL and 36 mg/mL, respectively.
2. We used 10-µL of PEGylated radioactive AuNPs and mixed with 10 µL of the EDC/NHS solution.
3. The new solution was then incubated for 30 minutes under room temperature.
4. We added 1 mL of PBS Tween (PBST) and vortex thoroughly.
5. The solution was centrifuged at 6,500 g for 30 min.
6. The supernatant was removed.
7. Added 10 µL of HIV-1 Tat (1 mg/mL in 1X PBS)
8. Sonicated in a water bath sonicator for 10 sec.

---

[i] http://www.cytodiagnostics.com/pdf/Covalent-conjugation-carboxyl-gold-nanoparticles-TECH_NOTE_105.pdf

9. Incubated for 2 to 4 hours at room temperature with mixing.
10. Added 1 mL of PBST and vortex thoroughly.
11. Spin down by centrifugation at 3,500 g for 30 min.
12. Removed most of the supernatant.
13. Added 50 μL PBS with 1% BSA.
14. Stored at 4 degrees until ready to use.

Once radioactive and non-radioactive AuNP are functionalized with HIV-1 Tat, they are ready to be used accordingly based on the arrangement described with RTCA system.

3. RESULTS

3.1 SKBr-3 RTCA Cell Seeding Experiments

In order to carry out our experiments with good growth of SKBr-3 over a period of time that is acceptable for observation without the need to change the growth medium, we carried out a cell seeding experiment. The RTCA system was used to assess the optimal seeding per well of SKBr-3 cells. Seeding densities were carried out at 3300, 5500, 10000, and 25000 cells per well. Figure 14 illustrates the cell index (CI) response as a function of time for a period of more than 190 h. The maximum CI achieved by these cells was estimated at 3.0 without exchanging the cell growth media.

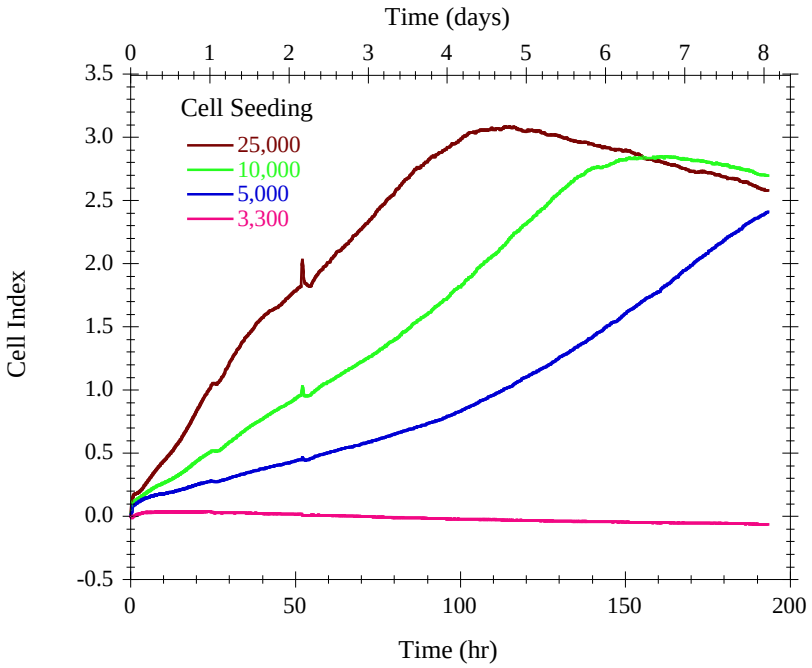

Figure 14. RTCA cell Index (CI) response as a function of time for seeding per well of 3,300 (pink), 5,000 (blue), 10,000 (green) and 25,000 (red) per well. The optimal seeding was determined at 10,000 cells per well within a time lapse of less than 196 h.

Based on these data, the optimal seeding was estimated at around 10,000 cells per well, reaching a CI of 1.5 within 84 h and allowing the assessment of potential cytotoxic response for CI < 1.5 or re-growth response for CI > 1.5. Based on these results, future experiments were carried out at a seeding of 10,000 cells per well.

3.2 Cytotoxicity of Doxorubicin on SKBr-3

For the purpose of evaluation and further comparison, the response of SKBr-3 to the chemotherapy drug doxorubicin was evaluated using the RTCA system. The mechanism of action of Doxil is by intercalating and inhibiting biosynthesis of topoisomerase II, which disrupts DNA synthesis.

We seeded 10,000 cells per well and allowed to them to grow for a period of 24 hours. Quadruplicates were used for each concentration and controls. The resulting RTCA response was dose dependent, as shown in Figure 15 where higher molar concentrations induced a rapid proliferation rate (higher CI) with a subsequent drop, which reveals that tumors cells continue to reproduce and grow after exposure. However, after several cell cycles cell death is inevitable via apoptosis, necrosis, autophagy, or mitotic catastrophe. The time required to achieve the same cell index (cross over) of controls for each molar concentration is shown in Figure 16, which indicates the inverse relationship between growth time reduction and molar concentration. This expression is similar to the dose-effect relationship laws used by different pharmacokinetic groups relation effect versus dose; however, in here time is used as a variable to assess the required time to inhibit continuous growth (35).

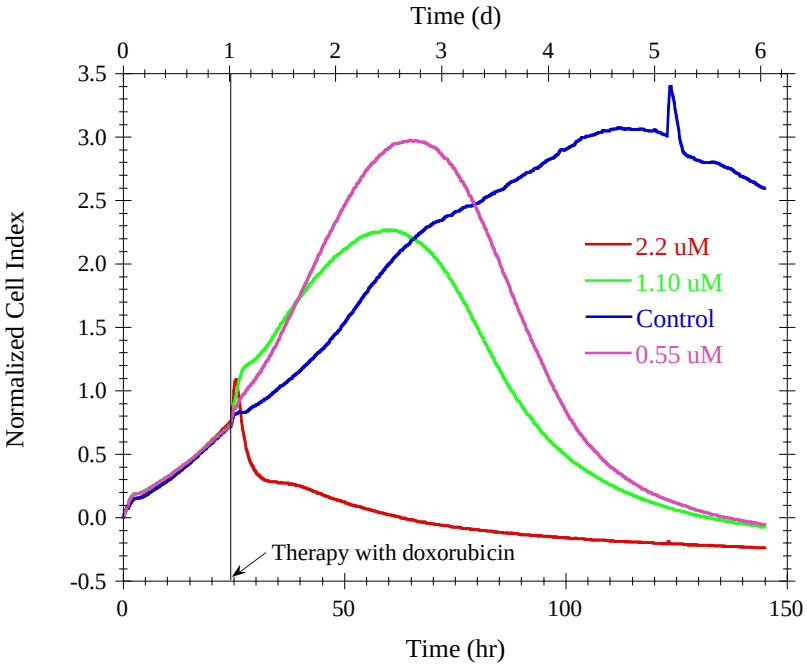

Figure 15. Cell index (CI) as a function of time for SKBr-3 cells exposed to different molar concentrations of doxorubicin. The molar concentrations were 2.2 µM (red), 1.10 µM (green), 0.55 µM (Pink), and controls (Blue). The solid black line represents the point at which the CI is normalized to unity when doxorubicin was given to the cells.

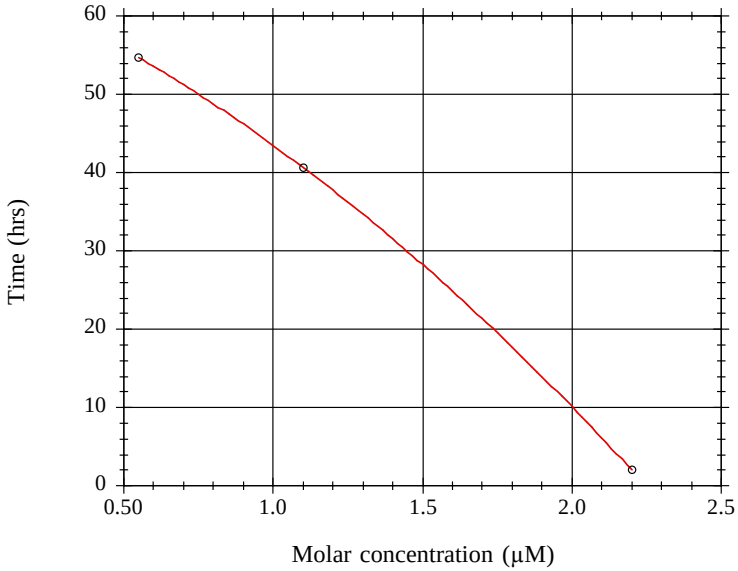

Figure 16. Time required achieving the same CI end-point (cross over) as a function of doxorubicin molar concentration.

3.3 Cytotoxicity of 2-Gy X-rays

The cytotoxic response to an absorbed dose of 2 Gy from photons (SF2Gy) is commonly used as a reference dose when comparing other therapies or cytotoxic modalities such as chemotherapy and radioimmunotherapy *in vitro*. Experiments were carried out using the RTCA system using two plates. Initially 10,000 cells per well were seeded and were allowed to grow for a period of 24 h. At the end of 24 h, one plate was irradiated with a total dose of 2 Gy while the other was used as a control. Figure 17 presents the CI response as a function of time. The CI was normalized at the time of irradiation (black reference line). We observed that SKBr-3 had an over-response, *i.e.*, a fast cell growth response, immediately after irradiation that lasted less than 24 h, reached a peak, and then declined to the same levels as controls due to cell death; possibly apoptosis. Growth media was replaced twice after irradiation. The observable effects of irradiation were seen after 147 h, where the CI for irradiated *versus* control differed significantly, by a factor of 3. These results demonstrate that cell death is not quite immediate after irradiation and that there are significant cell growth kinetic changes after irradiation, leading to a fast growth response followed by cell death only 60 h or more after irradiation.

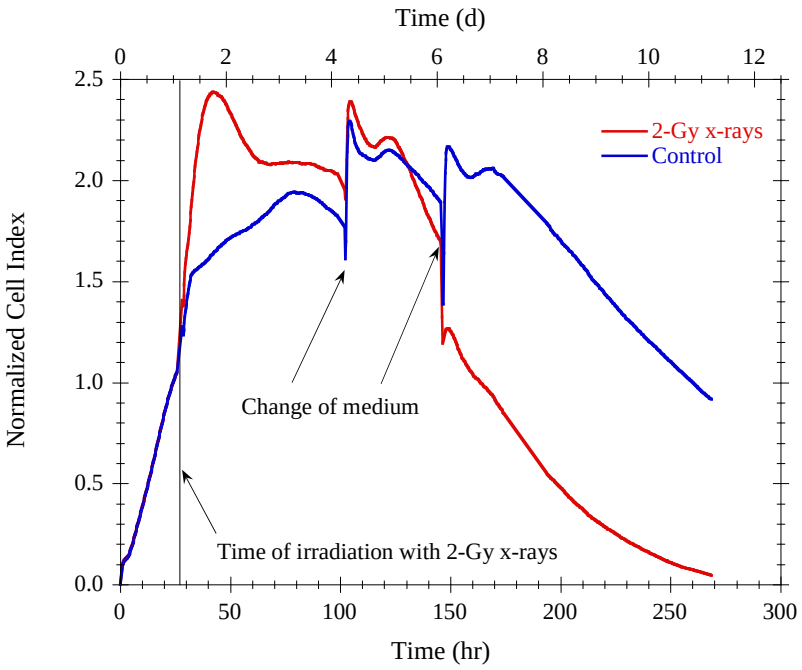

Figure 17. Normalized CI as a function of time for SKBr-3 cells exposed to 2 Gy (red line) and controls (blue line). The solid black line represents the point at which the CI is normalized to unity at the time of irradiation.

It was not clear if these results can be modeled using the Gompertz equation for cellular growth (36). What is of interest is the quasi-stable response of SKBr-3 for more than 50 h after irradiation, which indicates the death of multiple groups of cells at different times and rates. This may be due to the fact that cells are not synchronous (in different cell cycle phases) at the time of irradiation – because cells in the G_2/M phase (undergoing DNA synthesis) are likely to be more radiosensitive that those in the S/G_1 phase. When compared to the RTCA response of x-rays to that of doxorubicin, we observe similarities in cell proliferation immediate after exposure of the cytotoxic agent. However, for 2-Gy x-rays the time required to obtain a therapeutic response was more than 120 hours after exposure. In contrast, doxorubicin had a shorter therapeutic effect

after as a function of concentration. The obtained CI results were used to compare the cytotoxicity of doxorubicin, and functionalized ^{198}AuNP-HIV-1 Tat to SKBr-3 cells.

3.4 Characterization of ^{198}AuNPs

In order to characterize the produced radioactive gold nanoparticles, 1 ml of the resulting solution was used to assess the surface plasmon resonance using the NanoDrop 2000C spectrophotometer. Figure 18 shows the UV-Vis spectrum as a function of photon wavelength.

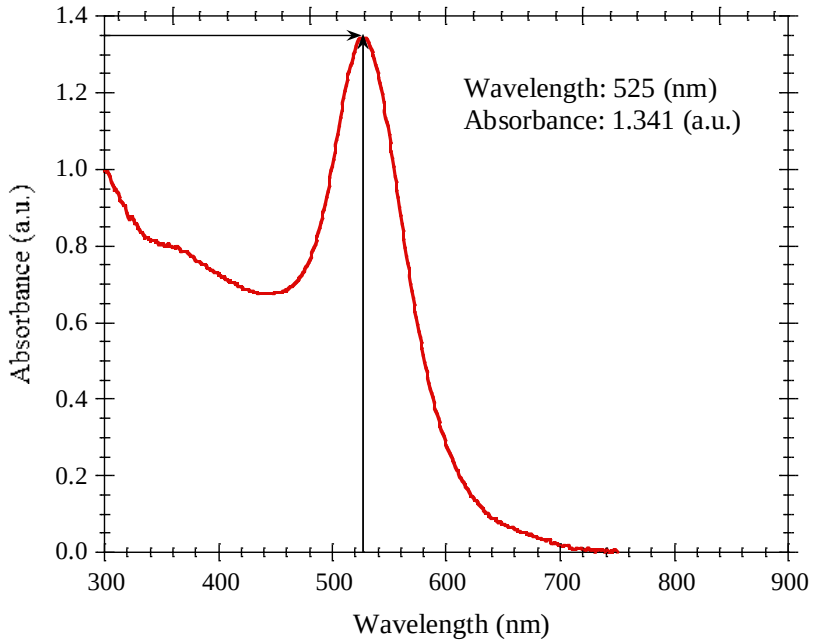

Figure 18. UV-Vis spectrum of radioactive gold nanoparticles produced for the present experiments. The surface plasmon resonance (maximum peak) was observed at 525 nm with an absorbance of 1.341 corresponding to a gold nanoparticle diameter of 32.9 nm and a concentration of 2.29×10^{11} NP/ml.

The absorbance peak was measured at 525 nm, which corresponded to particle size of 32.9 nm. The measured absorbance peak at 525 nm was 1.34 resulting in a concentration of 2.29×10^{11} (NP/ml). Using the dose calibrator, the measured activity of the 1 ml sample was 480 (μCi/ml). The estimated number of ^{198}Au atoms per nanoparticle was 25.9, which resulted in a negligible zero-fraction $\left(P\left(X=0\right)=e^{-25.9}\right)$.

3.5 Cytotoxicity of ^{198}AuNPs and ^{198}AuNPs-HIV-1 Tat

The cytotoxicity of radioactive ^{198}AuNPs was assessed using the RTCA system to corroborate its innocuous effect on SKBr-3. We seeded 10500 tumor cells per well and after 30 hours of incubation, HIV1-Tat functionalized and non-functionalized ^{198}AuNP with different activities were added into the wells in quadruplicates. The activities used were 50, 100, 500, 1000, and 1500 kBq. The experimental arrangement was as follow:

1. SKBr-3 cells used as a control
2. SKBr-3 cells treated with AuNPs (non-radioactive)
3. SKBr-3 cells treated with AuNP HIV-1 Tat (non-radioactive)
4. SKBr-3 cells treated with ^{198}AuNPs
5. SKBr-3 cells treated with ^{198}AuNP HIV-1 Tat

Figures 19 through 22 present the cell growth response as a function of time for the different experimental arrangements as described above. The incubation period was for 12 hours and after that the medium was exchanged and cells were washed once to

remove any non-internalized nanoparticles. However, it is important to mention that we were not able to determine the fraction of activity that was retained in the wells after washing them with PBS. We expected that internalization of ^{198}AuNPs-HIV-1 Tat will have a significant impact in cell growth; however, as observed in Figure 22, the growth profile of ^{198}AuNPs and ^{198}AuNPS-HIV-1 Tat was similar with a minimal reduction in cell index (CI) by those treated with ^{198}AuNPS-HIV-1 Tat. In here we question the effective internalization of ^{198}AuNPS-HIV-1 Tat and further studies are required to assess if internalization was 1) limited by nanoparticle size, 2) by number of HIV-1 Tat CPP per nanoparticle, 3) by radiation effects on cell cycle, or 4) lack of directionality of the HIV-1 Tat CPP against the cell surface. Nonetheless, we were able to observe a slight gain in cytotoxicity by the ^{198}AuNPs-HIV-1 Tat when compared with ^{198}AuNPs alone. The cell response to non-radioactive AuNPs-HIV-1 Tat was similar to that of controls as shown in Figure 19; this indicates that the non-radioactive AuNPs-HIV-1 Tat had no effect on the SKBr-3 cells growth.

In terms of activity, the cell growth response to 50, 100, and 500 kBq of ^{198}AuNPs and ^{198}AuNPs-HIV-1 Tat was not significant as shown in Figure 20 and 21; the cell growth response was similar to controls. However, the cell growth response to 1000 and 1500 kBq of ^{198}AuNPs and ^{198}AuNPs-HIV-1 Tat was observed distinctly. This shows that doses bellow 1000 kBq were too low to yield a cellular growth response.

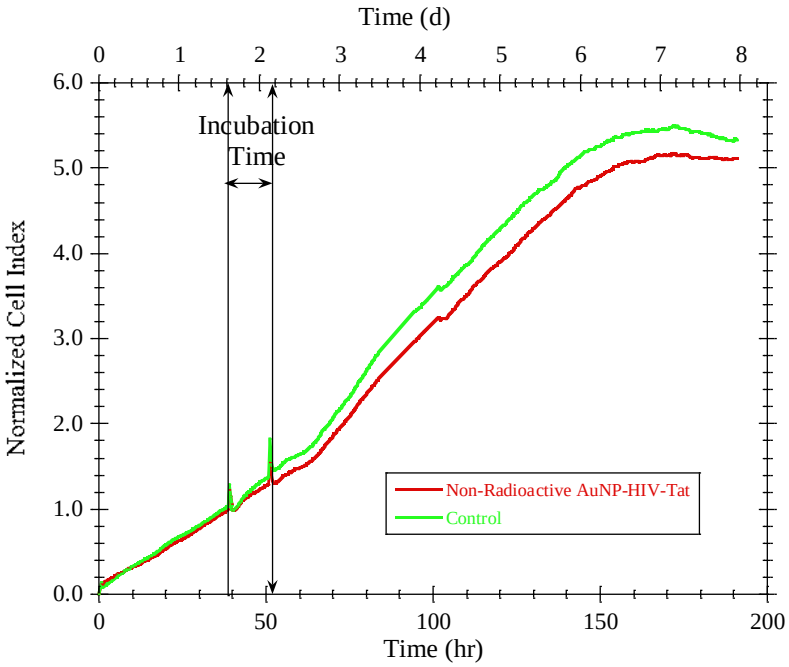

Figure 19. Normalized Cell Index as a function of time for SKBr-3 cells exposed to nonradioactive AuNP (green line) and control (red line). The solid black lines represent the incubation time between the addition of the AuNP and the time when the medium was replaced.

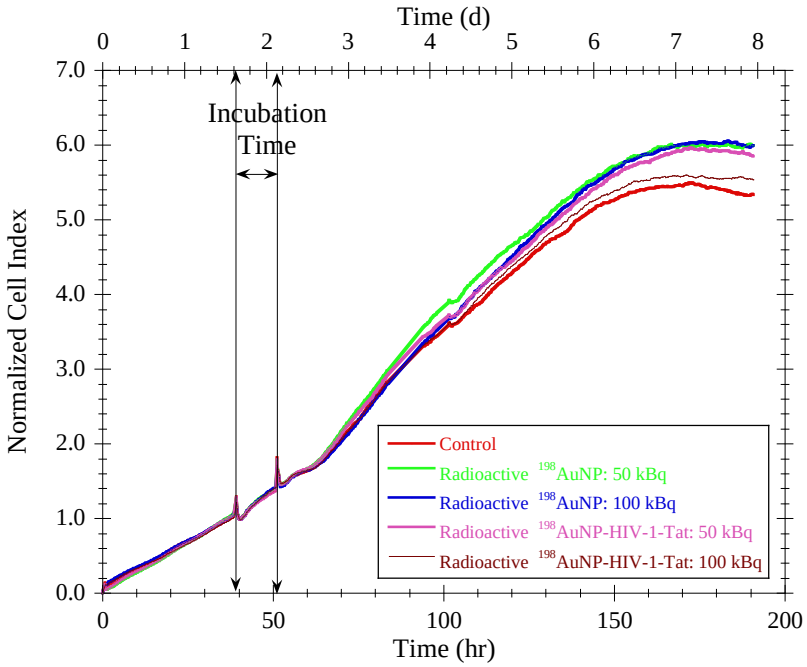

Figure 20. Normalized Cell Index as a function of time for SKBr-3 cells exposed to ^{198}AuNPs-HIV-1 Tat with an activity of 50 kBq (green line) and 100 kBq (blue line), ^{198}AuNPs with an activity of 50 kBq (pink line) and 100 kBq (brown line), and control (red line). The solid black lines represent the incubation time between the addition of the AuNP and the time when the medium was replaced.

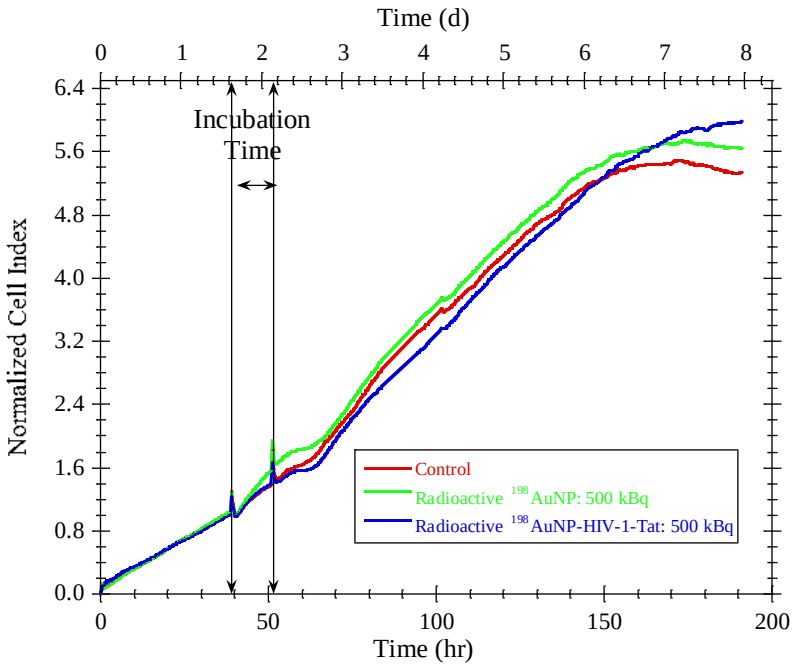

Figure 21. Normalized Cell Index as a function of time for SKBr-3 cells exposed to ^{198}AuNPs-HIV-1 Tat (green line) and ^{198}AuNPs (blue line) with an activity of 500 kBq and control (red line). The solid black lines represent the incubation time between the addition of the AuNP and the time when the medium was replaced.

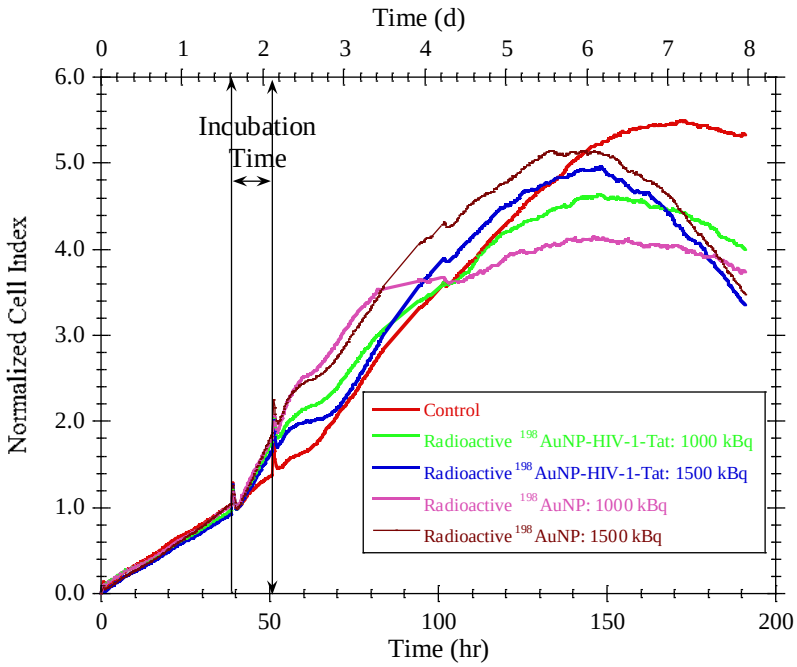

Figure 22. Normalized Cell Index as a function of time for SKBr-3 cells exposed to ^{198}AuNPs-HIV-1 Tat with an activity of 1000 kBq (green line) and 1500 kBq (blue line), ^{198}AuNPs with an activity of 1000 kBq (pink line) and 1500 kBq (brown line), and control (red line). The solid black lines represent the incubation time between the addition of the AuNP and the time when the medium was replaced.

The cell response to ^{198}AuNPs-HIV-1 Tat and ^{198}AuNPs with activities of 1000 and 1500 kBq was initially observed in the slope of the spectrum. Following the exchange of the medium inside the wells, a decrease in the slope was observed. This showed that the cells duplication rate was slowed as a function of time. The major observable effects of radioactive AuNP were seen after 150 h (~ 6 d), where the trend of the treated cells started declining with a very fast rate in cell death afterwards, while the trend of the controls kept growing reaching a plateau at 175 h (~ 7 d).

4. DISCUSSIONS

The biological functionalization of nanoparticles is an area of extensive research (37). The use of passive or active strategies for targeting tumors depends on the spatiotemporal pathophysiology of the tumor and the competitive processes embedded in the interaction and obstacles encountered by the nanoparticle/nanotherapeutic within the microenvironment of normal and tumor tissues. When delivering radioactive payloads, the design of a carrier will be based on the pathophysiology of the tumor itself. Passive strategies based on the enhanced permeability and retention effect (EPR) of tumors have been widely used with relative success in the treatment of prostate cancer using animal models (38). However, active strategies using immuno-conjugated monoclonal antibodies and their fragments, and tumor-directed cell penetrating peptides (39-43) are therapeutically more significant. This is because the EPR effect in small tumors is minimal or non-existent, which is the case for minimal residual disease and microscopic metastatic cancer. Therefore, preemptive active targeting strategies must be developed and studied to attack a tumor at its early stage of development before it becomes intractable, as is the case when tumors are radiographically observable.

In the present study we accomplished the production of ^{198}AuNPs using a modified Turkevich method and corroborated the NP size using TEM and UV-Vis. We assessed the cytotoxicity of x-rays for an absorbed dose of 2-Gy, which resulted in a very peculiar growth response as a function of time. What is of interest is the immediate growth response after irradiation, which is attributed to a morphological response by

increasing the cell surface attachment reaching a plateau and subsequent cell death, which was similar to controls for a period of approximately 24 hours. Subsequent to this time, the effect of irradiation becomes noticeable showing a decrease in cell index (CI) by a factor of 2.3 at 150 hours after irradiation between irradiated and controls. However, the rates (slopes) of cell death of irradiated and controls were almost identical. These results indicate that further research is required to assess if this effect is consistent and reproducible at higher absorbed doses (4 Gy and up). Nonetheless, the cytotoxicity of 2-Gy x-ray was obtained for further comparison with functionalized and non-functionalized ^{198}AuNPs.

We also assessed the cytotoxicity of the chemotherapy agent doxorubicin. Using the same SKBr-3 seeding of 10,000 cells per well and the same RTCA system settings at different molar concentrations. The immediate tumor growth response as a function of molar concentration was similar to that of 2-Gy x-ray irradiation. We observe a fast growth response for a short period of time with a subsequent decline by cell death; however, unlike the plateau response observed in x-rays, cell death continued and the CI declined in an exponential form as a function of time. This demonstrates that the mechanism of action and cell death pathways between ionizing radiation and chemotherapy may be completely different. It is clear that in both cases apoptosis may be the mechanism for cell death; however, cell death may be reached via different pathways that are completely unrelated by mechanism of action or activation of caspases, which can be either intrinsic (mitochondria mediated) or extrinsic (death receptor mediated). It is important also to point out that a 2-Gy absorbed dose was

delivered in a single dose providing a single event or insult to the SKBr-3 cell culture; on the other hand, doxorubicin was constantly present in the growth media of the SKBr-3 cell culture. This difference may account for observing the plateau response after immediate cell growth and cell death. It is important to mention that, in pharmacokinetic terms, radioactive ^{198}AuNP is a form of protracted irradiation similar to that chemotherapy agent but utilizes radiation (ionizing radiation, beta particles and photons) as a cytotoxic agent.

Furthermore, using the RTCA system found that bare non-radioactive AuNPs have negligible or no cytotoxicity on SKBr-3 cells. We used a very high concentration of AuNPs in these experiments and noticed no statistical difference in cell growth among the different well cultures and controls. This is of course an *in vitro* study using cell culture conditions; however, AuNPs may elicit a cytotoxic response under different growth conditions *in vivo*.

We also estimated the distribution of radioactive atoms per AuNP. The analysis required the calculation of the specific activity (*SA*), which was used to calculate the average number of radioactive ^{198}Au atoms per NP; we used the Poisson distribution to assess the fraction of NPs that will have zero, one, two, three, etc. radioactive atoms. This is important in the preparation of radioactive gold NPs. A very low *SA* will result in a large fraction of AuNPs containing no radioactive ^{198}Au atoms, whereas a high *SA* will results in a very optimal capacity of cell-kill as multiple radioactive decays at the same site within a tumor cell (either cell surface or cytoplasm) will occur yielding significant localized damage to the tumor cell.

The dosimetry of ^{198}AuNPs is extremely complex requiring the use of Monte Carlo transport methods for electrons and photons using a cellular phantom that mimics the internal components of a cell, including its membrane, cytoplasm, nucleus, including and cell replication. However, we presented the basis for the dosimetry of ^{198}AuNPs by organizing the corresponding radiative emissions (beta particles and characteristic electrons and x-rays) and probability distributions per decay (Bq-s) that need to be considered in these dosimetric calculations. However, we did not estimate the dose to the system an individual cell, as the system is very complex. A therapeutic effect was observed at 1000, and 1500 kBq per well but lower doses may be indicative of high radio-resistant of SKBr-3 cells.

In summary, results from the present study suggest that the effect of radioactive nanoparticles may be used as a potential strategy for the treatment of metastatic cancer based on the fact that a small response was observed at 1000, and 1500 kBq. If the pharmacokinetics of the present entity is optimal with a long residence time in blood, it may represent a potential opportunity to carry out chronic administrations of the present radiotherapeutic nanoparticle, yielding a management approach of metastatic cancer. Thus, further *in vitro* and *in vivo* investigations are warranted.

5. CONCLUSIONS

Novel potential cancer treatments can be attained by the synthesis of targeted radionuclide therapy (TRT) and nuclear nanotechnology. The use of nuclear nanotechnologies as a new paradigm where nanoparticle cores can serve as super-carriers of radionuclides may potentially yielding new endo-radiotherapy agents with potentially higher safety and efficacy profile than those currently used clinically. The use of nanoparticles as carriers of a therapeutic load was possible using gold-on-gold (^{198}Au-^{197}Au). Our method yielded good mono-dispersed AuNPs with an average diameter of 32.9 nm. We targeted tumor cells using the HIV-1 Tat cell penetrating peptide as an initial proof of principle. The cell growth results showed a clear dependence on administered activity and that cell growth response was only observable at 1000 and 1500 kBq per well for both functionalized and non-functionalized ^{198}AuNP. Even though an observable and distinct higher cytotoxic response was observed for those cells treated with ^{198}AuNP-HIV-1 Tat.

In summary, the use of ^{198}Au is a first step and it was used as a surrogate for other radionuclides. For future work, we propose to use nano-alloys as diagnostic and therapeutic agent such as the alpha particle emitting radionuclide, ^{211}At, for the treatment of metastatic cancer. Moreover, we propose the strategy of ^{68}Ga-AuNPs HIV1-Tat for PET diagnosis. The positron emitting radionuclide ^{68}Ga can be obtained using a ^{68}Ge/^{68}Ga generator.

REFERENCES

1. Stewart BW, Wild C, International Agency for Research on Cancer, World Health Organization. World cancer report 2014. Lyon, France Geneva, Switzerland: International Agency for Research on Cancer, WHO Press; 2014. xiv, 630 pages p.

2. SEER Cancer Statistics Review, 1975-2009 (Vintage 2009 Populations) [Internet]. National Cancer Institute. Bethesda, MD. 2012 [cited December 1st 2012]. Available from: http://seer.cancer.gov/csr/1975_2009_pops09/,.

3. Jones R, Jr., Jonsson U, Browning M, Lessner H, Price CC, Sen AK. Initial clinical trial of the nitrogen mustard analogues of chloroquine and quinacrine; a preliminary report. Annals of the New York Academy of Sciences. 1958 Apr 24;68(3):1133-50. PubMed PMID: 13627767.

4. Joiner M, Kogel Avd. Basic clinical radiobiology. 4th ed. London: Hodder Arnold; 2009. vi, 375 p.

5. Speer TW. Targeted radionuclide therapy. Philadelphia: Wolters Kluwer Health/Lippincott Williams & Wilkins; 2011. xvii, 537 p.

6. Baselga J, Arteaga CL. Critical update and emerging trends in epidermal growth factor receptor targeting in cancer. J Clin Oncol. 2005 Apr 10;23(11):2445-59. PubMed PMID: WOS:000228313200001. English.

7. Kaufman HL, Wolchok JD, SpringerLink (Online service). General principles of tumor immunotherapy : basic and clinical applications of tumor immunology; 2007. xii, 503 p.

8. Groner B. Targeted interference with signal transduction events. Berlin ; New York: Springer; 2007. ix, 188 p.

9. Sitaramayya A. Signal Transduction: Pathways, Mechanisms and Diseases. Signal Transduction: Pathways, Mechanisms and Diseases. 2010:1-436. PubMed PMID: WOS:000273693600024. English.

10. Bahnsen JS, Franzyk H, Sandberg-Schaal A, Nielsen HM. Antimicrobial and cell-penetrating properties of penetratin analogs: effect of sequence and secondary structure. Biochimica et biophysica acta. 2013 Mar;1828(2):223-32. PubMed PMID: 23085001. English.

11. Pao W, Miller VA. Epidermal growth factor receptor mutations, small-molecule kinase inhibitors, and non-small-cell lung cancer: current knowledge and future directions. J Clin Oncol. 2005 Apr 10;23(11):2556-68. PubMed PMID: 15767641.

12. Hammarstrom S. The carcinoembryonic antigen (CEA) family: structures, suggested functions and expression in normal and malignant tissues. Semin Cancer Biol. 1999 Apr;9(2):67-81. PubMed PMID: WOS:000080670800002. English.

13. Stohl W. B cell trophic factors and B cell antagonism in autoimmune disease. Basel ; New York: Karger; 2005. viii, 311 p.

14. Vokes EE, Weichselbaum RR. Concomitant Chemoradiotherapy - Rationale and Clinical-Experience in Patients with Solid Tumors. J Clin Oncol. 1990 May;8(5):911-34. PubMed PMID: WOS:A1990DB98600022. English.

15. Brizel DM, Vokes EE. Induction Chemotherapy: To Use or Not to Use? That Is the Question. Semin Radiat Oncol. 2009 Jan;19(1):11-6. PubMed PMID: WOS:000261524800003. English.

16. Salama JK, Haddad RI, Kies MS, Busse PM, Dong L, Brizel DM, et al. Clinical Practice Guidance for Radiotherapy Planning after Induction Chemotherapy in Locoregionally Advanced Head-and-Neck Cancer. Int J Radiat Oncol. 2009 Nov 1;75(3):725-33. PubMed PMID: WOS:000270573100013. English.

17. Bamrungsap S, Zhao ZL, Chen T, Wang L, Li CM, Fu T, et al. Nanotechnology in therapeutics: a focus on nanoparticles as a drug delivery system. Nanomedicine-Uk. 2012 Aug;7(8):1253-71. PubMed PMID: WOS:000307483000016. English.

18. De Villiers MM, Aramwit P, Kwon GS, SpringerLink (Online service). Nanotechnology in drug delivery. xiii, 662 pages, 18 unnumbered pages of plates p.

19. Lu WL, Qi XR, Zhang Q, Li RY, Wang GL, Zhang RJ, et al. A pegylated liposomal platform: Pharmacokinetics, pharmacodynamics, and toxicity in mice using doxorubicin as a model drug. J Pharmacol Sci. 2004 Jul;95(3):381-9. PubMed PMID: WOS:000222877100012. English.

20. National Research Council (U.S.). Committee on State of the Science of Nuclear Medicine. Advancing nuclear medicine through innovation. Washington, D.C.: National Academies Press; 2007. xiv, 159 p.

21. Dwivedi PD, Tripathi A, Ansari KM, Shanker R, Das M. Impact of Nanoparticles on the Immune System. J Biomed Nanotechnol. 2011 Feb;7(1):193-4. PubMed PMID: WOS:000291410800094. English.

22. Fadeel B. Clear and present danger? Engineered nanoparticles and the immune system. Swiss Med Wkly. 2012 Jun 26;142. PubMed PMID: WOS:000305801200003. English.

23. Fang RH, Hu CMJ, Zhang LF. Nanoparticles disguised as red blood cells to evade the immune system. Expert Opin Biol Th. 2012 Apr;12(4):385-9. PubMed PMID: WOS:000301457100001. English.

24. Zolnik BS, Gonzalez-Fernandez A, Sadrieh N, Dobrovolskaia MA. Minireview: Nanoparticles and the Immune System. Endocrinology. 2010 Feb;151(2):458-65. PubMed PMID: WOS:000273948600004. English.

25. Frankel AD, Pabo CO. Cellular uptake of the tat protein from human immunodeficiency virus. Cell. 1988 Dec 23;55(6):1189-93. PubMed PMID: 2849510.

26. Asai T, Tsuzuku T, Takahashi S, Okamoto A, Dewa T, Nango M, et al. Cell-penetrating peptide-conjugated lipid nanoparticles for siRNA delivery. Biochemical and Biophysical Research Communications. 2014 Mar 21;444(4):599-604. PubMed PMID: 24486551. English.

27. Lane HA, Motoyama AB, Beuvink I, Hynes NE. Modulation of p27/Cdk2 complex formation through 4D5-mediated inhibition of HER2 receptor signaling. Ann Oncol. 2001;12:21-2. PubMed PMID: WOS:000170999900005. English.

28. Franken NA, Rodermond HM, Stap J, Haveman J, van Bree C. Clonogenic assay of cells *in vitro*. Nat Protoc. 2006;1(5):2315-9. PubMed PMID: 17406473.

29. Kimling J, Maier M, Okenve B, Kotaidis V, Ballot H, Plech A. Turkevich method for gold nanoparticle synthesis revisited. J Phys Chem B. 2006 Aug 17;110(32):15700-7. PubMed PMID: WOS:000239656100012. English.

30. Kumar S, Aaron J, Sokolov K. Directional conjugation of antibodies to nanoparticles for synthesis of multiplexed optical contrast agents with both delivery and targeting moieties. Nat Protoc. 2008;3(2):314-20. PubMed PMID: 18274533.

31. Frens G. Controlled Nucleation for Regulation of Particle-Size in Monodisperse Gold Suspensions. Nature-Phys Sci. 1973;241(105):20-2. PubMed PMID: WOS:A1973O356200016. English.

32. Liu X, Atwater M, Wang J, Huo Q. Extinction coefficient of gold nanoparticles with different sizes and different capping ligands. Colloids and surfaces B, Biointerfaces. 2007 Jul 01;58(1):3-7. PubMed PMID: 16997536. English.

33. Schneider CA, Rasband WS, Eliceiri KW. NIH Image to ImageJ: 25 years of image analysis. Nature methods. 2012 Jul;9(7):671-5. PubMed PMID: 22930834.

34. Conde J, Ambrosone A, Sanz V, Hernandez Y, Marchesano V, Tian F, et al. Design of multifunctional gold nanoparticles for *in vitro* and *in vivo* gene silencing. ACS Nano. 2012 Sep 25;6(9):8316-24. PubMed PMID: 22882598.

35. Chou TC. Theoretical basis, experimental design, and computerized simulation of synergism and antagonism in drug combination studies. Pharmacological reviews. 2006 Sep;58(3):621-81. PubMed PMID: 16968952.

36. Moreno D, Troconiz IF, Enguita M, Bandres E, Garcia-Foncillas J, Garrido MJ. Semi-mechanistic description of the *in-vitro* antiproliferative effect of different antitumour agents. J Pharm Pharmacol. 2008 Jan;60(1):77-82. PubMed PMID: 18088508.

37. Jain KK. The handbook of nanomedicine. New York: Springer; 2012.

38. Torchilin V. Tumor delivery of macromolecular drugs based on the EPR effect. Adv Drug Deliv Rev. 2011 Mar 18;63(3):131-5. PubMed PMID: 20304019. Epub 2010/03/23. eng.

39. Jia L, Gorman GS, Coward LU, Noker PE, McCormick D, Horn TL, et al. Preclinical pharmacokinetics, metabolism, and toxicity of azurin-p28 (NSC745104) a peptide inhibitor of p53 ubiquitination - Springer. Cancer Chemotherapy and Pharmacology. 2011 Aug;68(2):513-24. PubMed PMID: 21085965. English.

40. Santini S, Bizzarri AR, Cannistraro S. Modelling the interaction between the p53 DNA-binding domain and the p28 peptide fragment of Azurin. Journal of Molecular Recognition. 2011;24(6):1043-55. PubMed PMID: 676838825810878556related:XGCmdlOdZAkJ.

41. Warso MA, Richards JM, Mehta D, Christov K, Schaeffer C, Rae Bressler L, et al. A first-in-class, first-in-human, phase I trial of p28, a non-HDM2-mediated peptide inhibitor of p53 ubiquitination in patients with advanced solid tumours. British Journal of Cancer. 2013 Apr 19;108(5):1061-70. PubMed PMID: 23449360. Pubmed Central PMCID: PMC3619084. English.

42. Yamada T, Christov K, Shilkaitis A, Bratescu L, Green A, Santini S, et al. p28, a first in class peptide inhibitor of cop1 binding to p53. British Journal of Cancer. 2013 Jul 25;108(12):2495-504. PubMed PMID: 23736031. Pubmed Central PMCID: PMC3694247. English.

43. Yamada T, Das Gupta TK, Beattie CW. p28, an anionic cell-penetrating peptide, increases the activity of wild type and mutated p53 without altering its conformation. Molecular pharmaceutics. 2013 Sep 03;10(9):3375-83. PubMed PMID: 23952735. English.